Long-term incubations provide insight into the mechanisms of anaerobic oxidation of methane in methanogenic lake sediments

Hanni Vigderovich[a], Werner Eckert[b], Michal Elul[a], Maxim Rubin-Blum[c], Marcus Elvert [d], Orit Sivan[a]

[a] Department of Earth and Environmental Science, Ben-Gurion University of the Negev, Beer Sheva, Israel

[b] Israel Oceanographic & Limnological Research, The Yigal Allon Kinneret Limnological Laboratory, Israel

[c] Israel Oceanographic & Limnological Research, Haifa, Israel

[d] MARUM - Center for Marine Environmental Sciences and Faculty of Geosciences, University of Bremen, Bremen, Germany

Corresponding author: Hanni Vigderovich, hannil@post.bgu.ac.il

Abstract

Anaerobic oxidation of methane (AOM) is among the main processes limiting the release of the greenhouse gas methane from natural environments. Geochemical profiles and experiments with fresh sediments from Lake Kinneret (Israel) indicate that iron-coupled AOM (Fe-AOM) sequesters 10-15% of the methane produced in the methanogenic zone (> 20-cm sediment depth). The oxidation of methane in this environment was shown to be mediated by a combination of *mcr* gene-bearing archaea and *pmoA* gene-bearing aerobic bacterial methanotrophs. Here, we used sediment slurry incubations under controlled conditions to elucidate the electron acceptors and microorganisms that are involved in the AOM process over the long term (~18 months). We monitored the process with the addition of ^{13}C-labeled methane and two stages of incubations: (i) enrichment of the microbial population involved in AOM and (ii) slurry dilution and manipulations, including the addition of several electron acceptors (metal oxides, nitrate, nitrite and humic substances) and inhibitors (2-bromoethanesulfonate, acetylene and sodium molybdate) of methanogenesis, methanotrophy and sulfate reduction/sulfur disproportionation. Carbon isotope measurements in the dissolved inorganic carbon pool suggest the persistence of AOM, consuming 3-8% of the methane produced at a rate of 2.0±0.4 nmol g^{-1} dry sediment day^{-1}. Lipid carbon isotopes and metagenomic analyses point towards methanogens as the sole microbes performing the AOM process by reverse methanogenesis. Humic substances and iron oxides, but not sulfate, manganese, nitrate, or nitrite, are the likely electron acceptors used for this AOM. Our observations support the contrast between methane oxidation mechanisms in naturally anoxic lake sediments, with potentially co-existing aerobes and anaerobes, and long-term incubations, wherein anaerobes prevail.

Keywords: Anaerobic oxidation of methane (AOM), lake sediments, dissolved inorganic carbon, stable carbon isotopes, electron acceptors, archaea, methanogens, methanotrophs, lipids.

1. Introduction

Methane (CH_4) is an important greenhouse gas (Wuebbles and Hayhoe, 2002), which has both anthropogenic and natural sources, the latter of which account for about 50% of the emission of this gas to the atmosphere (Saunois et al., 2020). Naturally occurring methane is mainly produced biogenically via the methanogenesis process, which is performed by methanogenic archaea. Traditionally acknowledged as the terminal process anchoring carbon remineralization (Froelich et al. 1979), methanogenesis occurs primarily via the reduction of carbon dioxide by hydrogen in marine sediments and via acetate fermentation in freshwater systems (Whiticar et al. 1986).

Methanotrophy, the aerobic and anaerobic oxidation of methane (AOM) by microbes, naturally controls the release of this gas to the atmosphere (Conrad, 2009; Reeburgh, 2007; Knittel and Boetius, 2009). In marine sediments, up to 90% of the upward methane flux is consumed anaerobically by sulfate, and in established diffusive profiles, that methane consumption occurs within a distinct sulfate-methane transition zone (Valentine 2002). While sulfate-dependent AOM, catalyzed by the archaeal ANaerobic MEthanotrophs (ANMEs) 1-3, is widespread chiefly in marine sediments (Hoehler et al., 1994; Boetius et al., 2000; Orphan et al., 2001; Treude et al., 2005, 2014), methane oxidation in other environments can be coupled to other electron acceptors (e.g. Raghoebarsing et al., 2006; Ettwig et al. 2010; Sivan et al., 2011; Crowe et al. 2011; Norði and Thamdrup 2014; Valenzuela et al., 2017).

In freshwater sediments, sulfate is often depleted, and methanogenesis may be responsible for most of the organic carbon remineralization, resulting in high concentrations of methane in shallow sediments (Sinke et al., 1992). Indeed, lakes and wetlands, are responsible for 33-55% of naturally emitted methane (Rosentreter et al., 2021). A large portion of this produced methane is oxidized by aerobic (type I, type II and type X) methanotrophic bacteria via oxygen. Aerobic methanotrophy is generally observed in the sediment-water interface (Damgaard et al. 1998) and/or in the water column thermocline (Bastviken 2009). AOM, however, can also consume over 50% of the produced methane (Segarra et al. 2015).

Sulfate can be an electron acceptor of AOM in freshwater sediments, as was shown for example in Lake Cadagno (Schubert et al., 2011, Su et al., 2020). Alternative electron acceptors for AOM in natural freshwater environments and cultures include humic substances, nitrate, nitrite and metals (such as iron manganese and chromium). Natural humic substances and their synthetic analogs were shown to function as terminal electron acceptors for AOM in soils, wetlands and cultures (Valenzuela et al., 2017; 2019; Bai et al., 2019; Zhang et al., 2019; Fan et al., 2020). Nitrate-dependent AOM has been demonstrated in a consortium of archaea and denitrifying bacteria from a canal (Raghoebarsing et al., 2006), in freshwater lake sediments (Norði and Thamdrup 2014) and a sewage enrichment culture of ANME-2d (Haroon et al., 2013; Arshad et al., 2015). Nitrite is exploited to oxidize methane by the

aerobic bacteria *Methylomirabilis* (NC-10), which split the nitrite to N_2 and O_2 and then uses the produced oxygen to oxidize the methane (Ettwig et al., 2010). ANME-2d were also suggested to be involved in Cr(VI) coupled AOM, either alone or with a bacterial partner (Lu et al., 2016). Iron and/or manganese coupled AOM have also been suggested in lakes (Sivan et al., 2011; Crowe et al. 2011; Norði et al., 2013), sometimes by supporting sulfate-coupled AOM (Shubert et al., 2011; Su et al., 2020; Mostovaya et al., 2021). Iron-coupled AOM was also shown to occur in enriched, denitrifying cultures from sewage where it was performed by ANME-2 (Ettwig et al. 2016), and in a bioreactor with natural sediments (Cai et al., 2018).

The mechanism and role of iron-coupled AOM in lake sediments have been studied with a variety of tools in the sediments of Lake Kinneret. *In-situ* pore water profiles and top core experiments (Sivan et al., 2011), diagenetic models (Adler et al., 2011) and batch incubation experiments with fresh sediment slurries (Bar-Or et al., 2017) suggest that iron coupled-AOM (Fe-AOM) removes 10-15% of the produced methane in the deeper part of the methanogenic zone (> 20 cm below the water-sediment interface). Analysis of the microbial community structure suggested that both methanogenic archaea and methanotrophic bacteria are potentially involved in methane oxidation (Bar-Or et al., 2015). Analyses of stable isotopes in fatty acids, 16S rRNA gene amplicons and metagenomics showed that both reverse methanogenesis by archaea and bacterial type I aerobic methanotrophy by Methylococcales play important role in methane cycling (Bar-Or et al., 2017; Elul et al., 2021). Aerobic methanotrophy, which has also been observed in the hypolimnion and sediments of several other lakes that are considered anoxic (Beck et al., 2013; Oswald et al., 2016; Martinez-Cruz et al., 2017; Cabrol et al., 2020), may be driven by the presence of oxygen at nanomolar levels (Weng et al., 2018). Pure cultures of the ubiquitous aerobic methanotrophs Methylococcales have indeed been shown to survive under hypoxia conditions either by oxidizing methane and with nitrate (Kits et al., 2015), by switching to iron reduction (Zheng et al., 2020), or even by exploiting their methanobactins to generate their own oxygen to fuel their methanotrophic activity (Dershwitz et al., 2021). The latter study also showed that the alphaproteobacterial methanotroph *Methylocystis* sp., strain SB2, can couple methane oxidation and iron reduction. However, whether these aerobic methanotrophic bacteria are able to oxidize methane under strictly anoxic conditions and which electron acceptors facilitate that activity are still not known.

In the current study, we used long-term anaerobic incubations to assess the dynamics of methane-oxidizing microbes under anoxic conditions and to quantify the respective availabilities of different electron acceptors for AOM. To that end, we diluted fresh methanogenic sediments from Lake Kinneret with original porewater from the same depth and amended the sediment with ^{13}C-labeled methane. Our experiment design comprised of two stages, the first of which included the enrichment of the microbial population involved in AOM, while the second involved an additional slurry dilution and several manipulations with different electron acceptors and inhibitors. We measured methane oxidation rates (based on ^{13}C-DIC enrichment), determined the characteristics of each electron acceptor (via its

105 turnover), and evaluated changes in microbial diversity over various incubation periods (based on
106 metagenomics and lipid biomarkers). The results from the long-term anaerobic incubations were
107 compared to those of batch and semi-continuous bioreactor experiments.

108 2. Methods

109 2.1 Study site

110 Lake Kinneret (Sea of Galilee) is a warm, monomictic, freshwater lake that is 21 km long and 13 km
111 wide and located in northern Israel. Its maximum depth is ~42 m at its center (station A, Figure S1)
112 while its average depth is 24 m. From March to December, the lake is thermally stratified, and from
113 April to December, the hypolimnion is anoxic. Surface water temperatures range from 15°C in the
114 winter (January) to 32°C in the summer (August), while the lake's bottom water temperatures remain
115 in the range of 14-17°C throughout the year. The sediment from the deep methanogenic zone used in
116 this study (sediment samples taken from a sediment depth of ~20 cm from the water-sediment interface
117 at the lake's center) contains 50% carbonates, 30% clay and 7% iron (Table S1). The dissolved organic
118 carbon (DOC) concentration of the porewater increases with depth, ranging from ~6 mg C L^{-1} at the
119 sediment-water interface to 17 mg C L^{-1} at a depth of 25 cm (Adler et al., 2011). The concentrations of
120 dissolved methane in the sediment porewater increase sharply with sediment depth, reaching a
121 maximum of more than 2 mM at a depth of 15 cm, after which the amounts of dissolved methane
122 gradually decreased with depth to 0.5 mM at a depth of 30 cm (Adler et al., 2011; Sivan et al., 2011;
123 Bar-Or et al., 2015).

124 2.2 Experimental setup

125 2.2.1 General

126 In this study we compared three incubation strategies (A, B and C; Fig. 1) in Lake Kinneret
127 methanogenic sediments (sediment depths > 20 cm), which were amended with original porewater from
128 the same depth, ^{13}C-labeled methane (0.05-2 ml; Table 1), different potential electron acceptors for
129 AOM (nitrite, nitrate, iron and manganese oxides and humic substances) and activity inhibitors. We
130 inhibited the *mcr* gene with 2-bromoethanesulfonate (BES), methanogenesis and methanotrophy with
131 acetylene, and sulfate reduction and sulfur disproportionation with Na-Molybdate (Nollet et al., 1997;
132 Oremland & Capone, 1988; Lovley & Klug, 1983). Below we describe the three incubation strategies
133 (Fig. 1).

134 A) Long-term, two-stage slurry incubations with a 1:1 sediment to porewater ratio and high methane
135 content for the first three months (first stage) to ensure the enrichment of the microorganisms involved
136 in AOM. After three months, the slurry was diluted with porewater to a 1:3 ratio (second stage) and
137 different reactants were added to the incubations, which were subsequently monitored for up to 18
138 months.

B) Semi-continuous bioreactor experiments in which sediments were collected up to three days before the experiment was set up (freshly sampled sediments). The sediment to porewater ratio was 1:4 and porewater was exchanged regularly.

C) Batch incubation experiments with freshly sampled sediments and porewater at a 1:5 ratio, respectively, and amended with hematite. This experimental set-up was described in our previous studies (Bar-Or et al., 2017; Elul et al., 2021).

The sediments for the slurries conducted in the current work were collected during seven day-long sampling campaigns aboard the research vessel *Lillian* between 2017 and 2019 from the center of the lake (Station A, Fig. S1) using a gravity corer with a 50-cm Perspex core liner. The length of the sediment in each core was 35-45 cm. During each sampling campaign, 1-2 sediment cores were collected for the incubations and 10 cores were collected for the porewater extraction. Sediments from the deeper methanogenic zone (sediment depths > 20 cm) for the experiments were diluted with porewater from the methanogenic zone of parallel cores sampled on the same day. The bottom part of the sediment cores (below 20 cm) was transferred, as a bulk, to a dedicated 5 L plastic container onboard. The cores and the container were brought back to the lab, where the cores were kept at 4°C, and the porewater was extracted on the same day of sampling. In the lab, sediments were collected from the container with 20-ml cutoff syringes and moved to 50-ml falcon tubes. The porewater was extracted by centrifugation at 9300 g for 15 min at 4°C, syringe filtered by 0.22-µM filters into 250-ml pre-autoclaved glass bottles, crimp-sealed with rubber stoppers, and flushed for 30 min with N_2. The extracted porewater was kept under anaerobic conditions at 4°C until its use. The sediments for the incubations were subsampled from the liners and diluted no later than three days after their collection from the lake and treated further according to the experimental strategies described above (setup A or B).

2.2.2 Experiment type A set-up: Long-term two-stage incubations (henceforth referred to as "two-stage" for simplicity)

Experiment A comprised ten two-stage incubation experiments (experiment serial numbers (SN) 1-10; Table 1) with different treatments (electron acceptors/shuttling/inhibitors). In the first stage (pre-incubation slurry), the sediment core was sliced under continuous N_2 flushing and sediments from depths > 20 cm were collected into zipper bags. The sediment was homogenized by shaking the sediment in the bag, and between 80-100 gr was transferred into 250-ml glass bottles under continuous N_2 flushing. The sediments were diluted with the extracted porewater to create a 1:1 sediment to porewater slurry with a headspace of 70-90 ml (Fig. 1). The slurries were sealed with rubber stoppers and crimped caps and were flushed with N_2 (99.999%, MAXIMA, Israel) for 30 min. Methane (99.99%, MAXIMA, Israel) was injected using a gas-tight syringe for a final content of 20% in the headspace, where 10% of the injected methane was ^{13}C-labeled methane (99%, Sigma-Aldrich). When significant

AOM activity was observed based on the increase of $\delta^{13}C_{DIC}$ after approximately three months (Fig. S2), some of the incubations were further diluted during the second stage of the experiments. The remainder of the incubations continued to be run with porewater exchange while the $\delta^{13}C_{DIC}$ values were monitored every three months.

All the experiments were set up similarly (see dates and detailed protocols in the supplementary information): the pre-incubation bottle was opened and subsamples (~18 g each) were transferred with a syringe and a Tygon® tube under a laminar hood and continuous flushing of N_2 gas into 60-ml glass bottles. The subsamples were then diluted with fresh anoxic porewater from the methanogenic zone (as described above) to achieve a 1:3 sediment to porewater ratio (Fig. 1) while leaving 24 ml of headspace in each bottle. The bottles were crimp-sealed, flushed with N_2 gas for 5 min, shaken vigorously and flushed again (3 times). Then ^{13}C-labeled methane was added to all of the bottles as described in Table 1. The "killed" control slurries in each experiment were autoclaved twice and cooled, only after which they were amended with the appropriate treatments and ^{13}C-labeled methane.

To the diluted (1:3) batch slurries electron acceptors were added either as a powder (hematite – experiment no. 1, magnetite – experiment no. 2, clay and humic substances – experiment no. 7, MnO_2 – experiment no. 3) or in dissolved form in double-distilled water (DDW) (KNO_3 – experiment no. 4, $NaNO_2$ – experiment no. 5). In addition, the potential involvement of sulfur cycling in the transfer of electrons was tested in experiment no. 2 via its inhibition with Na-molybdate (Lovley and Klug, 1983). The synthetic analog for humic substances, i.e., 9,10-anthraquinone-2,6-disulfonate (AQDS), was dissolved in DDW (detailed in the supplementary information) and added to the bottles of experiment no. 6 until a final concentration of 5 mM was achieved in each bottle. Amorphous iron ($Fe(OH)_3$) was prepared in the lab by dissolving $FeCl_3$ in DDW that was then titrated with NaOH 1.5 N up to pH 7 and injected into the bottles of experiment no. 2. The final concentration of each addition is detailed in Table 1. The ^{13}C-labeled methane was injected into all of the experimental bottles at the beginning of each experiment (unless described otherwise) by using a gas-tight syringe from a stock bottle filled with ^{13}C-labeled methane gas (which was replaced with saturated NaCl solution). Three different inhibitors were added to three different experiments: Molybdate was added to experiment No. 1 (to one bottle of methane-only treatment, magnetite treatment and amorphous iron treatment) to detect the feasibility of an active sulfur cycle; BES was added to experiment No. 8 at the start of the experiment; and acetylene was added to experiment No. 9, wherein it was injected during the experiment into two bottles at different timepoints after ^{13}C enrichment was observed in the DIC (Table 1).

All live treatments were set up in duplicate or triplicate, depending on the amount of the pre-incubated slurry aimed for each experiment, and the results are presented as the average with an error bar. In two experiments, only one "killed" control bottle was set up, and the remainder of the slurry was prioritized for other treatments because the killed controls repeatedly showed no activity in several previous

experiments. The humic substrate experiment used a natural (humic) substance that was extracted from a lake near Fairbanks, Alaska, where iron reduction was observed in the methanogenic zone. One experiment was set up without any additional electron acceptor to assess the rate of methanogenesis in the two-stage slurries. Porewater was sampled anaerobically for $\delta^{13}C_{DIC}$ and dissolved Fe(II) measurements in duplicate (2 ml), and methane was measured from the headspace. Variations in the $\delta^{13}C_{DIC}$ values between the experiments resulted from different amounts of ^{13}C-labeled methane injected at the start of each experiment (geochemical measurements detailed in the analytical methods section below).

2.2.3 Experiment type B setup: Semi-continuous bioreactor

Semi-continuous bioreactors were used to monitor the redox state regularly at close-to-natural *in-situ* conditions for 15 months in freshly collected sediments. Two 0.5-L semi-continuous bioreactors (Fig. 1) (LENZ, Weinheim, Germany) were set up with freshly sampled sediments from the methanogenic zone (25 - 40 cm) and extracted porewater from the same depth from Station A on Lake Kinneret immediately after their collection. Both reactors were filled, headspace-free, with a slurry at a 1:4 sediment to porewater ratio. One bioreactor was amended with 10 mM hematite while the second, which was a control, was not amended. To dissolve ^{13}C-labeled methane in the porewater, 15 ml of porewater were replaced with 15 ml of methane gas (13 ml of $^{12}CH_4$ and 2 ml of $^{13}CH_4$) to produce a methane-only headspace for 24 h, during which time the reactors were shaken repeatedly. After 24 h, the gas was replaced with anoxic porewater, thus eliminating the headspace, which resulted in lower methane concentrations (0.2 mM) than in either the two-stage incubations or the fresh batch experiment (~2 m). The redox potential was monitored continuously using a platinum/glass electrode (Metrohm, Herisau, Switzerland) to verify anoxic conditions and to determine the redox state throughout the incubation period. The bioreactors were subsampled weekly to bi-weekly, and the sample volume (5-10 ml) was replaced immediately by preconditioned anoxic (flushed with N_2 gas for 15 min) porewater from the methanogenic zone. As outlined below, samples were analyzed for dissolved Fe(II), methane and $\delta^{13}C_{DIC}$. Additional subsamples for metagenome and lipid analyses were taken at the beginning of the experiment and on days 151 and 382, respectively.

2.2.4 Experiment type C setup: Fresh batch experiment

Sediments for this experiment were collected in August 2013 at Station A using a protocol similar to that used to collect the sediments for the pre-incubations. Sediments from depths greater than 26 cm were diluted under anaerobic conditions with porewater from the same depth to obtain a ratio of sediment to porewater of 1:5. The resulting slurry was then divided between 60-ml glass bottles (40 ml slurry in each bottle). The sampling and experimental setup are described in detail in our earlier study (Bar-Or et al., 2017). Here we present our results of the $\delta^{13}C_{DIC}$, metagenome and lipid analyses of two treatments: natural (with only ^{13}C-labeled methane) and hematite. The experiment ran for 15 months.

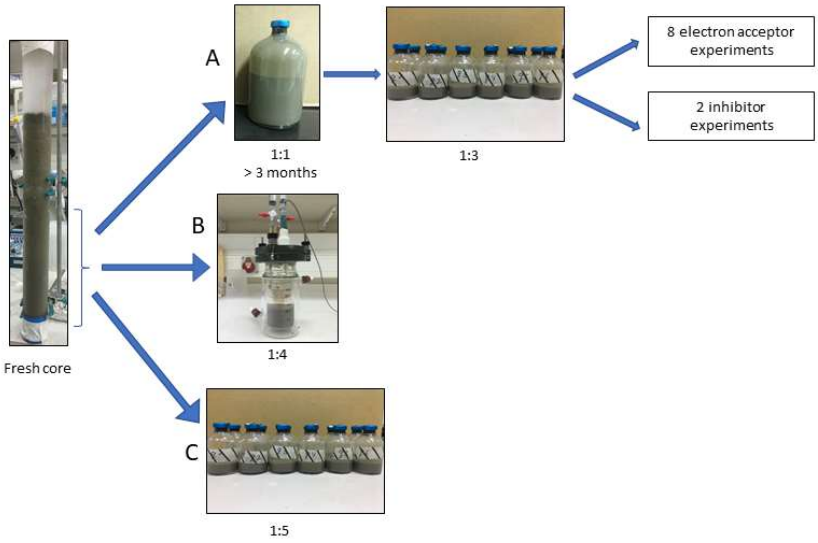

Figure 1: Flow diagram of the experimental design. Three types of experiments were set up to investigate the methanogenic zone sediments (deeper than 20 cm): **A)** Two-stage slurry experiments, with 1:1 ratio of sediment to porewater incubations and then with diluted pre-incubated slurries and porewater (1:3 ratio of sediment to porewater). **B)** Semi-continuous bioreactor experiment with freshly collected sediment. **C)** Fresh batch experiment – slurry experiment with freshly collected sediments (Bar-Or et al., 2017).

Table 1: Details of the three types of experiments: two-stage, semi-aerobic bioreactor and fresh batch experiments.

Experiment serial number (SN)	Experiment	Trearment	# of bottles	CH_4 [ml]	$^{13}CH_4$ [ml]	Fe_2O_3 [mM]	Fe_3O_4 [mM]	$Fe(OH)_3$ [mM]	MnO_2 [mM]	NO_2^- [mM]	NO_3^- [mM]	AQDS [mM]	Humic substances [mM]	PCA [mM]	Fe-bearing nontronite (clay) [gr]	Na_2-molybdate [mM]	BES [mM]	Acetylene [µL]	Temp [c°]	Duration [day]	Comments
1	Hematite	$^{13}CH_4$	2		1														20	201	
		$^{13}CH4$+hematite	2		1	10													20		
2	Magnetite	$^{13}CH_4$	2		1											1			16	447	The methane that was added at the beginning of the experiment was not labelled, so ^{13}C-labeled methane was added after 105 days. Na_2-molybdate was added to one of the bottles on day 365
		$^{13}CH_4$+magnetite	2		1		10									1			16		Na_2- molybdate was added to one of the bottles on day 365
		$^{13}CH_4$+$Fe(OH)_3$	2		1			10								1			16		
		Killed+ $^{13}CH_4$+magnetite	1		1		10												16		
3	MnO_2	$^{13}CH_4$	2		1.2														20	201	200 µL $^{13}CH_4$ was added on day 1, then another 1 mL was added on day 24.
		$^{13}CH_4$+MnO2	2		1.2				10										20		200 µL $^{13}CH_4$ was added on day 1, then another 1 mL was added on day 24.
4	Nitrate	$^{13}CH_4$+NO_3 (high conc.)	2	1	0.5	12					1								20	306	
		$^{13}CH_4$+hematite	2	1	0.5	12													20		
		$^{13}CH_4$+NO_3 (high conc.)+hematite	2	1	0.5	12					1								20		
		$^{13}CH_4$+NO_3 (low conc.)+hematite	2	1	0.5	12					0.2								20		
		Killed+ $^{13}CH_4$+NO_3^- (high conc.)+hematite	1	1	0.5	12					1								20		
5	Nitrite	$^{13}CH_4$	3	1	0.5														20	493	
		$^{13}CH_4$+NO_2^- (high conc.)+hematite	2	1	0.5	10				0.5									20		
		$^{13}CH_4$+NO_2^- (low conc.)+hematite	2	1	0.5	10				0.1									20		
		Killed+ $^{13}CH_4$+NO_2^- (high conc.)+hematite	2	1	0.5	10				0.5									20		
6	AQDS	$^{13}CH_4$	3		1														20	264	
		$^{13}CH_4$+AQDS	2		1							5							20		
		$^{13}CH_4$+AQDS+hematite	2		1	10						5							20		
		Killed+ $^{13}CH_4$+AQDS	2		1														20		
7	Natural humic acids and clay	$^{13}CH_4$	2		1														20	169	The head space of the experiment bottles was flushed with N_2 on day 51 and $^{13}CH_4$ was added. This was done in order to match the the clay bottles.
		$^{13}CH_4$+hematite	2		1	10													20		
		$^{13}CH_4$+humic acid	2		1								0.5						20		Clay was added on day 43, and the bottles were flushed again with N_2. $^{13}CH_4$ was added again on day 51.
		$^{13}CH_4$+clay	2		1										1				20		
		Killed+ $^{13}CH_4$+hematite	2		1	10													20		
8	Bromoethanesulfonate (BES)	$^{13}CH_4$+hematite	2	9	1	10													20	493	
		$^{13}CH_4$+hematite+BES	2	9	1	10											20		20		
9	Acetylene	$^{13}CH_4$+hematite	4	1	0.5	10												120	20	321	Acetylene was injected to each bottle at different time point doring the experiment.
		$^{13}CH_4$+hematite+acetylene	2	1	0.5	10												120	20		
		Killed+ $^{13}CH_4$+hematite	2	1	0.5	10													20		
10	No electron acceptor	No additions	3																20	147	
		$^{13}CH_4$	3		1														20		
	Semi-bioreactor	$^{13}CH_4$		13	2														16	345	
		$^{13}CH_4$+hematite		13	2	10													16	677	
	Freshly collected sediment exp.	$^{13}CH_4$			0.05														20	467	
		$^{13}CH_4$+hematite			0.05	20													20		

2.3 Analytical methods

2.3.1 Geochemical measurements

Measurements of $\delta^{13}C_{DIC}$ were performed on a DeltaV Advantage Thermo Scientific isotope-ratio mass-spectrometer (IRMS). Results are reported referent to the Vienna Pee Dee Belemnite (VPDB) standard. For these measurements, about 0.3 ml of filtered (0.22 µm) porewater was injected into a 12-ml glass vial with a He atmosphere and 10 µl of H_3PO_4 85% to acidify all the DIC species to CO_2 (g). The headspace autosampler (CTC Analytics; Type PC PAL) sampled the gas from the vials and measured the $\delta^{13}C_{DIC}$ of the sample on the GasBench interface with a precision of ±0.1 ‰. DIC was measured on the IRMS using the peak height and a precision of 0.05 mM. Dissolved Fe(II) concentrations were determined using the ferrozine method (Stookey, 1970) by HANON i2 visible spectrophotometer at a 562-nm wavelength with a detection limit of 1 µmol L^{-1}. A 100-µL headspace sample was taken for methane measurements with a gas-tight syringe and was analyzed by gas chromatograph (Focus GC, Thermo) equipped with a flame ionization detector (FID) and a packed column (Shincarbon ST) with a helium carrier gas (UHP) and a detection limit of 1 nmol methane. Bottles to which acetylene was added were also measured by the GC with the same column and carrier gas for ethylene to determine the acetylene turnover with the N cycle.

2.3.2 Lipid analysis

A sub-set of samples (Table 3) was investigated for the assimilation of ^{13}C-labeled methane into polar lipid-derived fatty acids (PLFAs) and intact ether lipid-derived hydrocarbons. A total lipid extract (TLE) was obtained from 0.4 to 1.6 g of the freeze-dried sediment or incubated sediment slurry using a modified Bligh and Dyer protocol (Sturt et al., 2004). Before extraction, 1 µg of 1,2-diheneicosanoyl-*sn*-glycero-3-phosphocholine and 2-methyloctadecanoic acid were added as internal standards. PLFAs in the TLE were converted to fatty acid methyl esters (FAMEs) using saponification with KOH/MeOH and derivatization with BF_3/MeOH (Elvert et al., 2003). Intact archaeal ether lipids in the TLE were separated from the apolar archaeal lipid compounds using preparative liquid chromatography (Meador et al., 2014) followed by ether cleavage with BBr_3 in dichloromethane forming hydrocarbons (Lin et al., 2010). Both FAMEs and ether-cleaved hydrocarbons were analyzed by GC-mass spectrometry (GC-MS; Thermo Finnigan Trace GC coupled to a Trace MS) for identification and by GC-IRMS (Thermo Scientific Trace GC coupled via a GC Isolink interface to a Delta V Plus) to determine $\delta^{13}C$ values by using the column and temperature program settings described by Aepfler et al. (2019). The $\delta^{13}C$ values are reported with an analytical precision better than 1‰ as determined by long-term measurements of an *n*-alkane standard with known isotopic composition of each compound. Reported fatty acid isotope data are corrected for the introduction of the methyl group during derivatization by mass balance calculation similar to equation 1 (see below) using the measured $\delta^{13}C$ value of each FAME and the known isotopic composition of methanol as input parameters.

289 2.3.3 Metagenomic analysis

290 For the metagenomic analyses, total genomic DNA was extracted from the semi-aerobic bioreactor with
291 hematite addition (duplicate samples), pre-incubation slurries ($^{13}CH_4$-only control, $^{13}CH_4$ + hematite)
292 and their respective initial slurries (t0) by using the DNeasy PowerLyzer PowerSoil Kit (QIAGEN).
293 Genomic DNA was eluted using 50 µl of elution buffer and stored at −20 °C. Metagenomics libraries
294 were prepared at the sequencing core facility at the University of Illinois at Chicago using the Nextera
295 XT DNA library preparation kit (Illumina, USA). Between 19 and 40 million 2 × 150 bp paired-end
296 reads per library were sequenced using Illumina NextSeq500. Metagenomes were co-assembled from
297 the concatenated reads of all of the metagenomic libraries with Spades V3.12 (Bankevich et al., 2012;
298 Nurk et al., 2013) after decontamination, quality filtering (QV= 10) and adapter-trimming with the
299 BBDuk tool from the BBMap suite (Bushnell B, http://sourceforge.net/projects/bbmap/). Downstream
300 analyses, including reading coverage estimates, automatic binning with maxbin (Wu et al., 2014) and
301 metabat2 (Kang et al., 2019) bin refining with the DAS tool (Sieber et al., 2018), were performed within
302 the SqueezeMeta framework (Tamames and Puente-Sánchez, 2019). GTDB-Tk was used to classify the
303 metagenome-assembled genomes (MAGs) based on Genome Taxonomy Database release 95 (Parks et
304 al., 2021). The principal component analysis biplot was constructed with Past V4.03 (Hammer et al.,
305 2001).

306 2.3.4 Rate calculations

307 Methanogenesis rates were calculated from temporal changes in methane concentration in a
308 representative pre-incubated slurry experiment (Fig. 2). The amount of methane oxidized was calculated
309 by a simple mass balance calculation according to equations 1 and 2:

310 $$x \times F^{13}CH_4 + (1 - x) \times FDI^{13}C_i = FDI^{13}C_f \quad (1)$$

311 $$[CH_4]_{ox} = x \times [DIC]_f \quad (2)$$

312 The final DIC pool comprises two end members, the initial DIC pool and the oxidized ^{13}C-CH_4. The
313 term *x* denotes the fraction of oxidized ^{13}C-CH_4, while 1-*x* denotes the fraction of the initial DIC pool
314 out of the final DIC pool. $F^{13}CH_4$ is the fraction of ^{13}C out of the total CH_4 at t0 (i-initial), $FDI^{13}C_i$ is
315 the fraction of ^{13}C out of the total DIC at t0, and $FDI^{13}C_f$ is the fraction of ^{13}C out of the total DIC at
316 t-final. $[CH_4]_{ox}$ is the amount (concentration in pore water) of the methane oxidized throughout the full
317 incubation period, and $[DIC]_f$ is the DIC concentration at t-final. It was assumed that the isotopic
318 composition of the labeled CH_4 did not change significantly throughout the incubation period.

319 ## 3. Results

320 In ten sets of slurry incubation experiments, we followed the progress of the methane oxidation process
321 in Lake Kinneret methanogenic sediments in type A two-stage long-term incubations. This is by

monitoring the changes in $\delta^{13}C_{DIC}$ values and by running metagenomic and specific isotope lipid analyses. We also followed methane oxidation in a semi-continuous bioreactor system (type B) with freshly collected sediments with or without the addition of hematite (Fig. 3). The results were compared to those of fresh batch slurry incubations (type C) from the same methanogenic zone, presented by Bar-Or et al. (2017) and Elul et al. (2021).

3.1 Geochemical trends in the long-term two-stage experiments

In the second stage (1:3 ratio of sediment to porewater) long-term batch slurry experiments (type A) from the methanogenic zone, methanogenesis occurred with net methanogenesis rates of ~ 25 nmol g dry weight $(DW)^{-1}$ d^{-1} (Fig. 2, Table S2), which are similar to those of fresh incubation experiments (Bar-Or et al., 2017). At the same time there was a conversion of ^{13}C-methane to ^{13}C-DIC in all the non-killed slurries amended with ^{13}C-methane, indicating AOM (Figs. 3 and 4). The $\delta^{13}C_{DIC}$ values of the "methane-only" control slurries reached as high values as 743‰. The average AOM rate in the methane-only controls was 2.0±0.4 nmol g DW^{-1} d^{-1} (Table 2). AOM was observed in these geochemical experiments also with the addition of electron acceptors, and the potential of several electron acceptors to perform and stimulate the AOM process is detailed below.

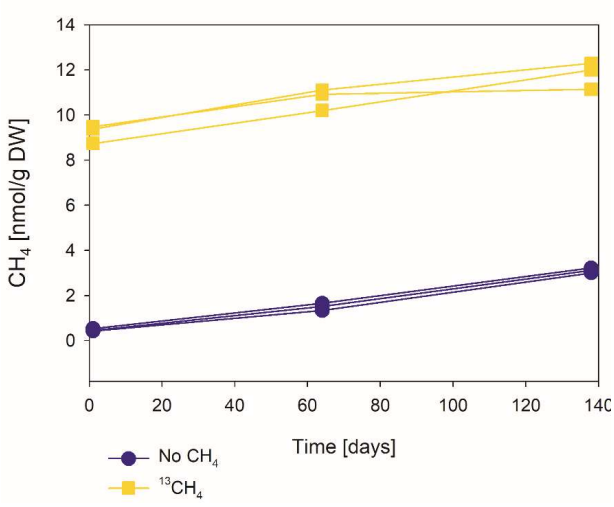

Figure 2: The change of methane concentrations with the time of a representative incubated second stage long-term slurry experiment, showing apparent net methanogenesis with the average rate of 25 nmol g DW^{-1} d^{-1}.

3.1.1 Metals as electron acceptors

Iron and manganese oxides were added as potential electron acceptors to the second-stage long-term slurries. The addition of hematite to three different experiments increased the $\delta^{13}C_{DIC}$ values over time to 694‰, similar to the behavior of the methane-only controls, and in a different pattern than the fresh experiments (Fig. 3). The average AOM rate in those two-stage treatments was 1.0±0.3 nmol g DW^{-1}

d^{-1} (Table 3). Magnetite amendments resulted in a minor increase of $\delta^{13}C_{DIC}$ values compared to the methane-only controls (200‰ and 265‰, respectively, Fig. 4A) with an AOM rate of 1.8 nmol g DW^{-1} d^{-1}. Amorphous iron amendments resulted in only a 22‰ increase in $\delta^{13}C_{DIC}$ and a lower AOM rate (0.1 nmol g DW^{-1} d^{-1}, Fig. 4A and Table 2). The addition of iron-bearing clay nontronite did not cause any increase in the $\delta^{13}C_{DIC}$ values (Fig. 4B), but the concentration of dissolved Fe(II) increased compared to the natural methane-only control (Fig. 5). Based on $\delta^{13}C_{DIC}$ estimates, no AOM was detected 200 days after the addition of MnO_2 whereas the $\delta^{13}C_{DIC}$ values of the methane-only controls increased to over 500‰ (Fig. 4F).

3.1.2 Sulfate as an electron acceptor

The involvement of sulfate in the AOM in the incubations was tested, even in the absence of detectable sulfate in the methanogenic sediments. This is as sulfate could theoretically still be a short living intermediate for the AOM process in an active cryptic sulfur cycle (Holmkvist et al., 2011). It was quantified directly by adding Na-molybdate to the methane-only controls and the magnetite amended treatments in the second stage long-term incubations (Fig. 4A). The addition of Na-molybdate did not affect the increasing trend of $\delta^{13}C_{DIC}$ with time, and therefore, the AOM rates remained unchanged, similar to the observation in the fresh batch incubations (Bar-Or et al., 2017).

3.1.3 Nitrate and nitrite as electron acceptors

Nitrate and nitrite involvement in the AOM was tested for the feasibility of an active cryptic nitrogen cycle, even in the absence of detectable amounts of nitrate and nitrite in the sediments (Nüsslein et al., 2001; Sivan et al., 2011). Nitrate was added at two different concentrations (0.2 and 1 mM, Fig. 4C) to the second stage long-term slurries amended with hematite, as these concentrations were shown previously to promote AOM in other settings (Ettwig et al., 2010). The addition of hematite alone increased the $\delta^{13}C_{DIC}$ values by ~200‰ during the 306 days of the experiment. The $\delta^{13}C_{DIC}$ in the bottles with the addition of 1 mM nitrate, with and without hematite (Fig. 4C; the data points of the two treatments are on top of each other), decreased from 43‰ at the beginning of the experiment to 35‰ after 306 days. The $\delta^{13}C_{DIC}$ in the bottles with the addition of 0.2 mM nitrate and hematite increased by 27‰ at the end of the experiment. Following the addition of 0.5 mM of nitrite, we observed no increase in $\delta^{13}C_{DIC}$ values during the first 222 days (Fig. 4D), after which they increased from 34‰ to 54‰ by the end of the experiment. The AOM rate of the high nitrite concentration treatment was 0.2 nmol g DW^{-1} d^{-1} (Table 2). Following the addition of 0.1 mM nitrite, $\delta^{13}C_{DIC}$ increased only after 130 days to 158‰ on day 493. The AOM rate of the low nitrite concentration treatment was 0.5 nmol g DW^{-1} d^{-1}. In the methane-only controls, the $\delta^{13}C_{DIC}$ value reached a maximum of 330‰.

3.1.4 Organic compounds as electron acceptors

Two of the second stage long-term incubation experiments were amended with synthetic and natural organic electron acceptors to test the potential of organic electron acceptors. The addition of AQDS to slurries with and without hematite caused a decrease in $\delta^{13}C_{DIC}$ values over the entire duration of the experiment (Fig. 4E). Dissolved Fe(II) increased by 50 µM in these treatments, while in those without AQDS, it exhibited an increase of 20 µM (Fig. S3). We further tested the effect of naturally occurring humic substances by using those isolated from a different natural lake. The results show that the $\delta^{13}C_{DIC}$ values did not change at the beginning of the experiments (Fig. 4B), while a steep increase of ~90 µM in their Fe(II) concentration was observed (Fig. 5). After 20 days, the $\delta^{13}C_{DIC}$ values of these slurries started to increase dramatically from 84‰ to 150‰ with an AOM rate of 1.2 nmol g DW^{-1} d^{-1} (Fig. 4B, Table 2). Dissolved Fe(II) concentrations mirrored the trend of $\delta^{13}C_{DIC}$ with a steep increase during the first 20 days followed by a decrease of 37 µM (Fig. 5).

3.1.5 Metabolic pathways

To elucidate which metabolic processes drive AOM, we analyzed $\delta^{13}C_{DIC}$ following the addition of inhibitors to the second stage long-term slurries: i) BES, a specific inhibitor for methanogenesis (Nollet et al., 1997) and ii) acetylene, a non-specific inhibitor for methanogenesis and methanotrophy (Orembland and Capone, 1988). In both cases and similar to the killed control, labeled ^{13}C-DIC production was completely inhibited following the addition (Fig. 6). Though acetylene can also inhibit nitrogen cycling in some cases, it has been shown to result in the production of ethylene (Oremland and Capone, 1988). In our case, however, no ethylene was detected, supporting the conclusion that only the methanogenesis activity was inhibited.

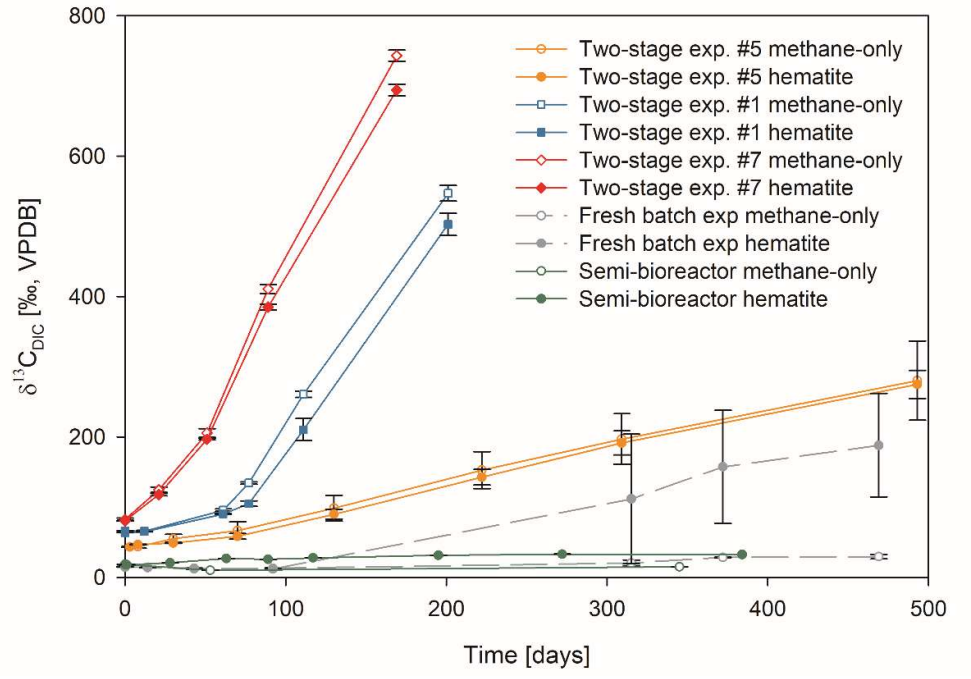

399 Figure 3: Comparison of $\delta^{13}C_{DIC}$ values among the three types of experiments with ^{13}C -labeled methane addition:
400 A) three two-stage slurry experiments (at the second stage of 1:3 ratio of sediment to porewater); B) the semi-
401 continuous bioreactor experiment; and C) slurry batch experiment with freshly collected sediments (Bar-Or et al.,
402 2017). In each experiment, two treatments are shown, with hematite (filled symbol) and without hematite (empty
403 symbols). The error bars represent the average deviation of the mean of duplicate/triplicate bottles.

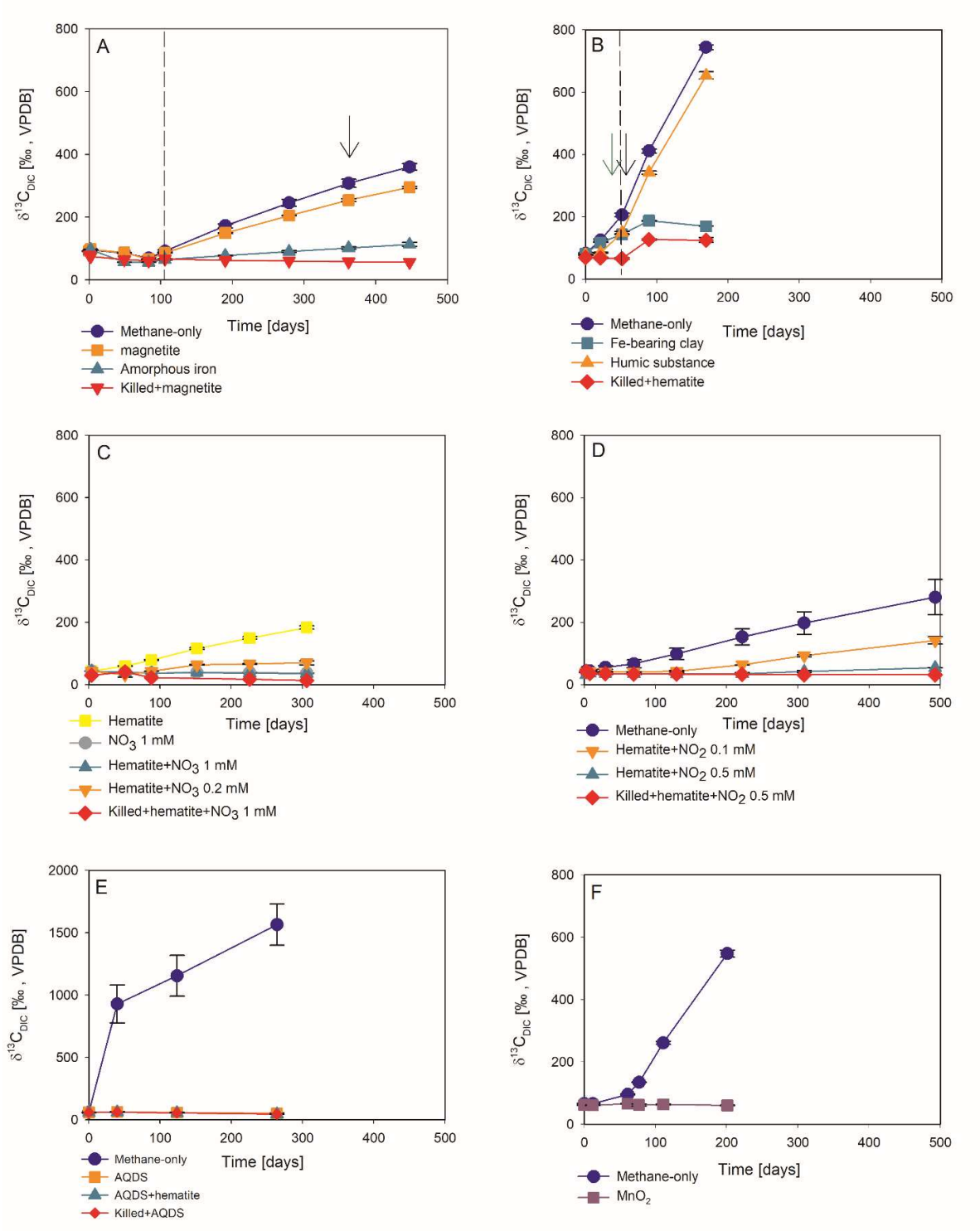

404

405 Figure 4: Potentials of different electron acceptors for AOM in Lake Kinneret in the two-stages long-term slurry
406 experiments (at the second stage of 1:3 ratio of sediment to porewater) with of ^{13}C -labeled methane and the
407 following treatments: (A) with and without the addition of magnetite and amorphous iron ($Fe(OH)_3$). The dashed
408 line represents the specific time of ^{13}C -labeled methane addition. The black arrow represents the addition of Na-
409 molybdate as an inhibitor for sulfate reduction. (B) with clay and natural humic substance. The green arrow
410 represents the time clay was added to the relevant bottles, the dashed line represents the time the headspace of
411 each bottle was flushed again with N_2, and the black arrow represents the second injection of 1 mL of ^{13}C-labeled
412 methane. (C) with the addition of hematite and two different concentrations of nitrate. (D) with the addition of
413 hematite and two different concentrations of nitrite. (E) with the addition of AQDS. (F) with and without the
414 addition of ^{13}C-labeled methane to all the bottles (see Table 1 for specific experimental details). Error bars
415 represent the average deviations of the data points from their means of duplicate/triplicate bottles.

416 Table 2: AOM rates and AOM role in experiment type A second stage slurries amended with ^{13}C-labeled methane
417 and different electron acceptors (assuming methanogenesis rate of 24.8 nmol g DW^{-1} d^{-1}).

Experiment serial number (SN)	Treatment	AOM rate [nmol/g DW X d]	AOM/methanogenesis [%]
10	**methane only**	1.1	4.4
1	**methane only**	1.6	6.4
	methane+hematite	0.5	2.1
2	**methane only**	2.4	8.2
	methane+magnetite	1.8	6.3
	methane+amorphous iron	0.1	0.5
7	**methane only**	1.4	6.4
	methane+hematite	1.3	6.0
	methane+humics	1.2	5.4
5	**methane only**	1.0	4.6
	methane+hematite	1.0	4.6
	methane+hematite+nitrite 0.5 mM	0.2	0.8
	methane+hematite+nitrite 0.1 mM	0.5	2.1

418

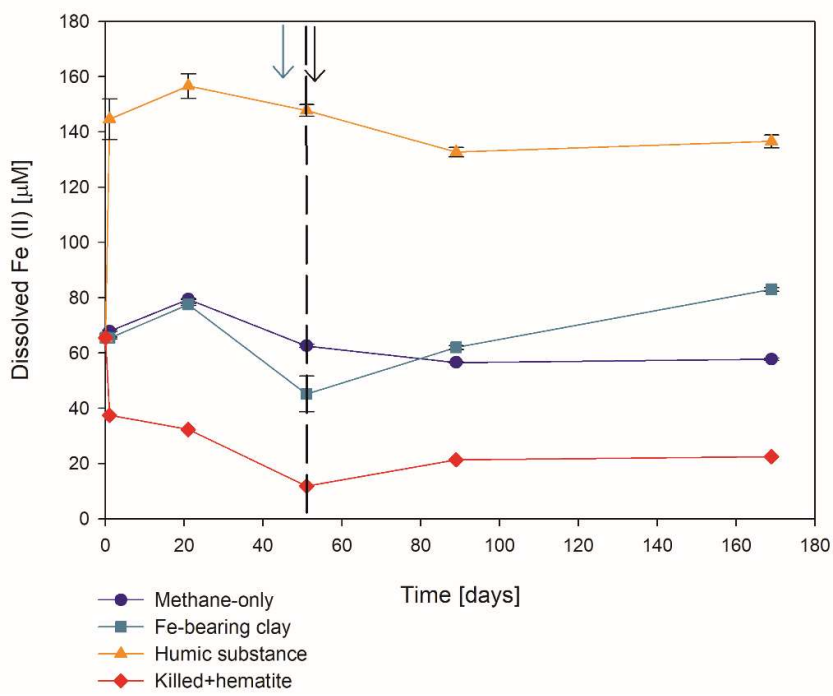

Figure 5: Change in dissolved Fe(II) in the second stage of experiment No. 7 containing clay and natural humic acid. The green arrow represents the time at which clay was added to the specific bottles and those bottles were flushed with N_2, the dashed line represents the time at which the rest of the bottles were flushed, and the black arrow represents the time at which ^{13}C-labeled methane was added again. Error bars represent the average of the absolute deviations of the data points from their means.

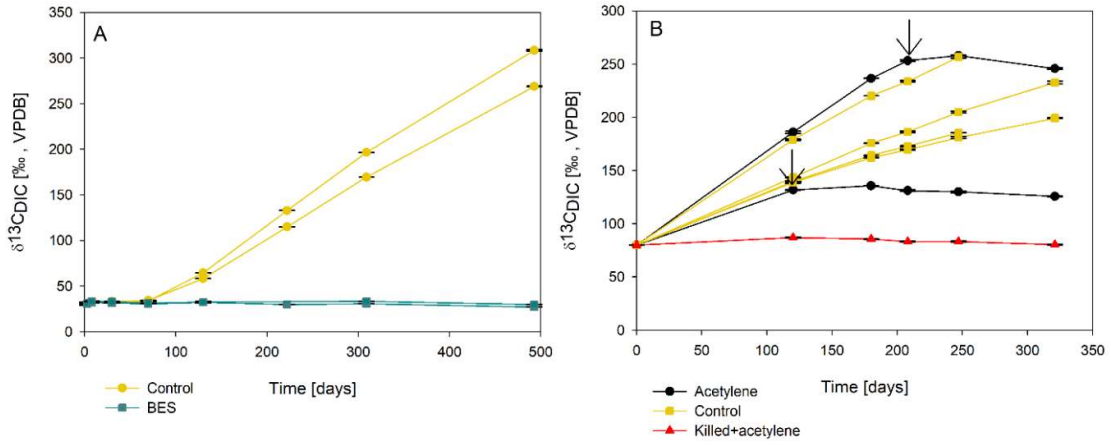

Figure 6: Change in $\delta^{13}C_{DIC}$ values over time in the second stage long-term sediment slurry incubations amended with hematite and ^{13}C-labeled methane. (A) with/without BES and (B) with/without acetylene. Black arrows represent the time at which acetylene was injected into the experiment bottle. The error bars are smaller than the symbols.

3.2 Microbial dynamics

Analyses of taxonomy and coverage of metagenome-assembled genomes suggest that in the pre-incubated two-stage slurries, Bathyarchaeia are the dominant archaea, together with putative methanogens such as Methanofastidiales (Thermococci), Methanoregulaceae (Methanomicrobia) and Methanotrichales (Methanosarcina) (Supplementary coverage table). Bona-fide ANME (ANME-1) were detected with substantial coverage of approximately 1 (the 27th most abundant from among the 195 MAGs detected) in all of the treatments. Among the bacteria, the sulfate reducers Desulfobacterota and Thermodesulfovibrionales (Nitrospirota) were prominent together with the GIF9 Dehalococcoida lineage, which is known to metabolize chlorinated compounds in lake sediments (Biderre-Petit et al., 2016). Some Methylomirabilales (NC10) were found (average coverage of 0.32±0.06), and no Methanoperedens were detected. Methylococcales methanotrophs were found in the natural sediments and the fresh batch and bioreactor incubations (average of 0.34±0.02), in contrast to their average coverage of 0.09±0.04 in the long-term incubations. Methylococcales comprised the *Methyloterricola*, *Methylomonas* and *Methylobacter* genera (Supplementary coverage table). The methylotrophic partners of aerobic methanotrophs, *Methylotenera*, were found in fresh batch and bioreactor incubations, where *Methylomonas* was found, findings that are in line with those of previous studies that showed their association (Beck et al., 2013). Principal component analysis shows the grouping of long-term, pre-incubated slurries, semi-aerobic bioreactor incubations, and fresh batch experiments (Fig. 7), emphasizing the microbial dynamics over time.

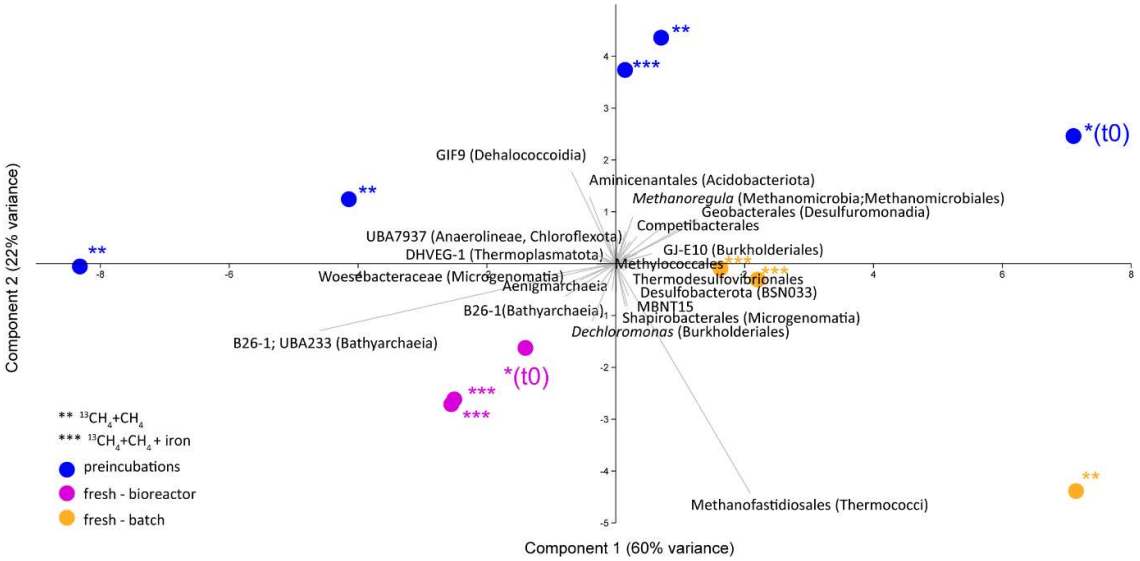

Figure 7: Principal component analysis comparison of three types of samples: long-term pre-incubated slurries (blue – experiment A), semi-continuous bioreactor (pink – experiment B) and fresh batch experiments (orange – experiment C). One asterisk represents t0, two asterisks denote methane-only treatments, three asterisks represent hematite treatment.

3.3 Lipid analysis

The $\delta^{13}C$ values of the archaeol-derived isoprenoid phytane were between −5 and −17‰ in the long-term pre-incubated samples and thus showed ^{13}C-enrichment of 15 to 27‰ relative to the original sediment. This is indicative of methane-derived carbon assimilation by archaea (Table 3). Acyclic biphytane, derived mainly from caldarchaeol, exhibited a less pronounced ^{13}C-enrichment of 5-10‰. For bacterial-derived fatty acids, $\delta^{13}C$-values similarly shifted by up to 10‰ relative to the original sediment. Nonetheless, one would have expected much higher values if aerobic methanotrophs were active, as was previously indicated by strong ^{13}C-enrichments of up to 1,650‰ in $C_{16:1\omega5c}$ observed in freshly incubated batch samples (Bar-Or et al., 2017).

Table 3: The $\delta^{13}C$ values (in ‰) of fatty acids and isoprenoid hydrocarbons from different experiments compared to values obtained from the original sediment in the methanogenic zone.

			Fatty acids		Hydrocarbons	
Description	Temperature (°C)	Sampling (days)	$C_{16:1\omega9/8/7}$	$C_{16:1\omega5}$	Phytane	Biphytane
Pre-incubated slurry +$^{13}CH_4$+hematite	20	411	-40	-43	-17	-23
Pre-incubated slurry +$^{13}CH_4$ (bottle A)	20	411	-40	-43	-13	-24
Pre-incubated slurry +$^{13}CH_4$ (bottle B)	20	1227	-36	-41	-5	-38
[a] Fresh batch experiment+$^{13}CH_4$+hematite	20	470	610	1600	-14	-28
Semi-bioreactor+$^{13}CH_4$+hematite	16	382	n.d.	n.d.	n.d.	n.d.
Original sediment (28-30 cm)	14		-44	-51	-32	-33

[a] Bar-Or et al., 2017
n.d. – Not detected

4. Discussion

4.1 Anaerobic oxidation of methane in the methanogenic sediment incubation experiments

The *in-situ* geochemical and microbial diversity profiles (Bar-Or et al., 2015) and the geochemical (Sivan et al., 2011; Bar-Or et al., 2017; Fig. 3) and metagenomic (Elul et al., 2021) analyses of batch incubations with fresh sediments provided strong support for the occurrence of Fe-AOM in sediments of the methanogenic zone below 20 cm. Such profiles and alongside incubations showed an unexpected presence of aerobic bacterial methanotrophs together with anaerobic microorganisms, such as methanogens and iron reducers (Adler et al., 2011; Sivan et al., 2011; Bar-Or et al., 2015; Bar-Or et al., 2017; Elul et al., 2021). These findings suggested that both *mcr* gene-bearing archaea and aerobic bacterial methanotrophs mediate methane oxidation. In the current study, we have supportive evidence of considerable AOM in the long-term incubations, even after the two treatment stages and considering the low abundance of the microbial populations.

The data from the second stage incubations show a similar increasing trend in the $\delta^{13}C_{DIC}$ values of both natural (methane-only) and the hematite amended treatments (Fig. 3). This deviates from our observations during experiments B and C with fresh sediment, wherein higher $\delta^{13}C_{DIC}$ values were

obtained after the addition of hematite than in the methane-only treatment (Fig. 3 and Bar-Or et al. (2017)). This was particularly dramatic in the batch slurries (experiment C), but it was also observed in the semi-continuous bioreactor (experiment B). We assume that the observed difference in the bioreactors would have been more pronounced if methane concentrations had been higher, but it is still a relevant finding. We also note that the difference between the bioreactors results may also be due to the fact that each bioreactor community developed separately. The results of the type A experiments (compared to those of types B and C) suggest that either hematite lacks the potential to stimulate the AOM activity during the two-stage experiments or that there is enough natural Fe(III) in the sediments to sustain the maximum potential of Fe-AOM. Below we characterize the AOM process in the long-term, two-stage incubation experiments.

4.2 Potential electron acceptors for AOM in the long-term two-stage incubation experiments

4.2.1 Metal oxides as electron acceptors

Measurements of $\delta^{13}C_{DIC}$ show that the additions of magnetite, amorphous iron, clays and manganese oxide in the second stage incubations resulted in a less pronounced increase in the $\delta^{13}C_{DIC}$ values compared to those of the methane-only controls (Fig. 4). A possible explanation for the latter may be that these metal oxides inhibit AOM, either directly or via a preference for organoclastic iron reduction over Fe-AOM, which adds a natural, more negative carbon isotope signal from the organic materials rather than the heavy carbon from the ^{13}C-labeled methane. Using mass-balance estimations in the methane-only and in the amorphous iron treatments and considering the DIC concentrations and $\delta^{13}C_{DIC}$ values of the methane-only treatments at the beginning of the experiment (6 mM and 60‰, respectively) and the values at the end (6.5 mM and 360‰, respectively), about 0.5 mM of the DIC was added by the AOM of methane with $\delta^{13}C$ of ~4000‰. The DIC and $\delta^{13}C_{DIC}$ values of the amorphous iron treatment at the beginning of the experiment were 5.4 mM and 60‰, respectively, and by the end were 6.1 mM and 120‰, respectively. Assuming the same $\delta^{13}C$ of the added methane of 4000‰ and a $\delta^{13}C_{TOC}$ of −30‰ (Sivan et al., 2011), 0.1 mM of the DIC should derive from AOM and 0.6 mM from organoclastic metabolism. This means that adding amorphous iron to the system encouraged iron reduction that was coupled to the oxidation of organic compounds other than methane. Intrinsic microbes, particularly the commonly detected ex-deltaproteobacterial lineages such as Geobacterales, may catalyze Fe(III) metal reduction, regardless of AOM (Xu et al., 2021). Manganese oxides are found in very low abundance in Lake Kinneret sediments (0.1 %, Table S1 and Sivan et al., 2011). Thus, their role in metal-AOM is likely minimal.

4.2.2 Sulfate as an electron acceptor

Sulfate concentrations in the methanogenic Lake Kinneret sediments have been below the detection limit in years past, similar to their representation in the natural sediments we used for the incubations

(< 5 μM, Bar-Or et al., 2015; Elul et al., 2021). Sulfide concentrations have also been reported to be minor (< 0.3 μM, Sivan et al., 2011). However, sulfate could theoretically still be a short-lived intermediate for the AOM process, as pyrite and FeS precipitate in the top sediments, and cryptic cycling via pyrite or FeS may replenish the sulfate, thus rendering it available for AOM (Bottrell et al., 2000). The addition of Na-molybdate to the second stage slurries, including those amended with and without magnetite, did not change the $\delta^{13}C_{DIC}$ dynamics, which remained similar to those from before the addition of the inhibitor (Fig. 4A). This finding is in line with that in fresh batch sediment slurries (Bar-Or et al., 2017) and suggests that sulfate is not a potent electron acceptor for AOM in this environment. Furthermore, although sulfate-reducing bacteria were abundant, none of the reducers belonged to the known clades of ANME-2d partners, which were connected previously to the Fe-S-CH_4 coupled AOM (Su et al., 2020; Mostovaya et al., 2021).

4.2.3 Nitrogen species as electron acceptors

Nitrate and nitrite concentrations are also undetectable in the porewater of Lake Kinneret sediments (Nüsslein et al., 2001; Sivan et al., 2011), but again may appear as short-lived intermediate products of ammonium oxidation that is coupled to iron reduction (Tan et al., 2021; Ding et al., 2014; Shrestha et al., 2009; Clement et al., 2005). We thus assessed the roles of nitrate and nitrite as electron acceptors in the two-stage slurries. Our results indicate that the addition of nitrate did not promote AOM, likely due to the absence of ANME-2d, which is known to use nitrate (Arshad et al., 2015; Haroon et al., 2013). In the case of nitrite, even low concentrations appeared to delay the increase in $\delta^{13}C_{DIC}$ values, suggesting that organoclastic denitrification outcompetes AOM, and despite the occurrence of Methylomirabilia, the role of nitrite-AOM is not prominent in the two-stage incubations (Figs. 4C, D).

4.2.4 Humic substances as electron acceptors

Humic substances may promote AOM by continuously shuttling electrons to metal oxides (Valenzuela et al., 2019). Though humic substances were not measured directly in Lake Kinneret sediments, the DOC concentrations in the methanogenic depth porewater were previously found to be high (~1.5 mM, Adler et al., 2011), suggesting that they may play a role in AOM. Compared to the methane-only treatments, the treatment with the synthetic humic analog AQDS caused an increase in dissolved Fe(II) concentrations, but it did not cause ^{13}C-DIC enrichment. This may be explained by the behavior of AQDS as a strong electron shuttle in organoclastic iron reduction (Lovely et al., 1996), which produces isotopically more negative carbon that masks the AOM signal (Fig. 4E, Fig. S3). Yet, as was done by Valenzuela et al. (2017), the addition of natural humic substances did promote AOM, compared to the rest of the electron acceptors tested, and may thus support AOM (Fig. 4B). In our incubations, the natural humic substances promoted first the oxidation of organic matter by iron reduction, probably by shuttling electrons from the broad spectrum of organic compounds to natural iron oxides (Figs. 4B and

5). When the availability of the iron oxides or the organic matter decreased, humic substances likely took over to facilitate the AOM (Fig. 4B).

Overall, the results of our long-term two-stage experiments indicate that sulfate, nitrate, nitrite and manganese oxides do not support AOM in the methanogenic sediments of Lake Kinneret. The candidate electron acceptors for AOM in the long-term experiments are natural humic substances and/or naturally abundant iron minerals. Future experiments can simulate iron limitation and the involvement of iron oxides in the AOM by removing natural iron oxides from the sediments.

4.3 Main microbial players in the long-term two-stage slurries

Methane oxidation in the pre-incubated Lake Kinneret sediments is likely mediated by either ANMEs or methanogens, as the addition of BES and acetylene immediately stopped the AOM (Fig. 6) similar to the results of the killed bottles and the BES treatment in the fresh batch experiment (Bar-Or et a., 2017). Apart from methane-metabolizing, acetylene can inhibit nitrogen cycling, which results in ethylene production (Oremland and Capone, 1988). This was not the case in our incubations, as no ethylene was produced. The increase in $\delta^{13}C$ values in phytane and biphytane (Table 3) also indicates the presence of active archaeal methanogens or ANMEs (Wegener et al., 2008; Kellermann et al., 2012; Kurth et al., 2019).

Using the isotopic compositions of specific lipids and metagenomics, we identified a considerable abundance of aerobic methanotrophs and methylotrophs in the fresh sediments, but not in the long-term slurries (Table 3, Fig. 7). In the natural sediments, micro levels (nano molar) of oxygen could be trapped in clays and slowly released to the porewater (Wang et al., 2018). However, if such micro levels of oxygen still existed during the time of the pre-incubation, they were probably already exhausted. Indeed, the results of our specific lipids and metagenomics analyses suggest that the aerobic methanotrophs lineages play only a minor role in the long-term slurries, probably due to complete depletion of the oxygen. The metagenomic data (Fig. 7, Supplementary coverage table) also indicate that Bathyarchaeia, which may be involved in methane metabolism (Evens et al., 2015), were enriched in the bioreactor incubations, yet their role in Lake Kinneret AOM remains to be evaluated. We also observed changes in the abundance of bacterial degraders of organic matter and necromass: for example, GIF9 Dehalococcoidia, which can metabolize complex organic materials under methanogenic conditions (Cheng et al., 2019; Hug et al., 2013), were most abundant in the long-term incubations (Fig. 7, Supplementary coverage table). Though ANME-1 are likely mediators of AOM in these sediments, methane oxidation via reverse methanogenesis is feasible for some methanogens in Lake Kinneret sediments (Elul et al., 2021).

4.4 Mechanism of methane oxidation in the long-term two-stage incubations

Our results indicate net methanogenesis in the two-stage incubation experiments with an average rate of 25 nmol g^{-1} DW day^{-1} (Fig. 1 and Table S2), which are similar to those from fresh incubation experiments (Bar-Or et al., 2017). This is despite the overall trend of increasing $\delta^{13}C_{DIC}$ values, a result representing potential methane turnover (Figs. 3 and 4). A likely explanation for the presence of both signals is an interplay between methane production and oxidation, which is possibly triggered by reversal of the methanogenesis pathway in bonafide ANMEs or certain methanogens (Hallam et al., 2004; Timmers et al., 2017). Due to the overall production of methane and the lack of intense stimulation of AOM by any electron acceptor added, the increase in $\delta^{13}C_{DIC}$ values could theoretically result from the occurrence of carbon back flux during methanogenesis, which is feasible in environments that are close to thermodynamic equilibrium (Gropp et al., 2021). To test this, we used DIC mass balance calculations to determine the strength of back flux in our incubations. Based on equations 1 and 2, the observed level of ^{13}C-enrichment indicates that 3-8% of the ^{13}C-methane should be converted into DIC. These estimates are orders of magnitude higher than the previously reported values of 0.001-0.3% for methanogenesis back flux in cultures (Zehnder and Brock, 1979; Moran et al., 2005), but they are in the same range as the back flux of 3.2 to 5.5% observed in ANME-enrichment cultures (Holler et al., 2011). For the latter, however, modeling approaches from AOM-dominated marine sediment samples and associated ANME enrichment cultures indicated the absence of net methanogenesis (Yoshinaga et al., 2014; Chuang et al., 2019; Meister et al., 2019; Wegener et al., 2021). Thus, it seems unlikely that back flux alone can account for the methane-to-DIC conversion in Lake Kinneret sediments. Moreover, the occurrence of back flux alone in marine methanogenic sediments with similar net methanogenesis rates and abundant methane-metabolizing archaea did not yield considerable ^{13}C-enrichment in the DIC pool following sediment incubations (Sela-Adler et al., 2015; Amiel, 2018; Vigderovich et al., 2019; Yorshansky, 2019) (Table S3). It is, therefore, less likely that the observed DIC values in our study were sustained by methanogenesis back flux alone (without an external electron acceptor) than by active AOM, which, in this case, is probably performed by ANME-1 or by methanogens, with the latter performing reverse methanogenesis to some extent.

Conclusions

Previous results of geochemical and microbial profiles as well as incubations with fresh sediments from Lake Kinneret constitute evidence of the occurrence of Fe-AOM in the methanogenic zone. The process is performed by anaerobic archaeal methanogens and bacterial methanotrophs, which remove about 10-15% of the methane produced in the lake's sediment. In the current study, we found that after two incubation stages and intensive purging for a prolonged duration, AOM was still significant, consuming 3-8% of the methane produced. However, the abundance of aerobic methanotrophs decreased and anaerobic archaea (ANME-1 or specific methanogens) appeared to be solely responsible for methane turnover. AOM could be a result of carbon back flux, as the methanogenic/AOM pathway is reversible,

however, the high $\delta^{13}C_{DIC}$ signal points to a metabolic reaction. Terminal electron acceptors or electron shuttles stimulating Fe-AOM are either hematite and/or humic substances. The role of the aerobic methanotrophs of the order *Methylococcales*, which were found in the freshly collected sediment experiments, remains to be examined.

Competing interests. The authors declare that they have no conflict of interest.

Acknowledgments

We would like to thank B. Sulimani and O. Tzabari from the Yigal Allon Kinneret Limnological Laboratory for their onboard technical assistance. We thank all of O. Sivan's lab members for their help during sampling and especially heartfelt thanks to N. Lotem for the invaluable assistance with the mass balance calculations and the fruitful discussions and E. Eliani-Russak for her technical assistance. Many thanks to K. Hachmann from M. Elvert's lab for his help during lipid analysis and to J. Gropp for insightful discussions about the back flux. This work was supported by ERC consolidator (818450) and Israel Science Foundation (857-2016) grants awarded to O. Sivan. Funding for M. Elvert was provided by the Deutsche Forschungsgemeinschaft (DFG) under Germany's Excellence Initiative/Strategy through the Clusters of Excellence EXC 309 'The Ocean in the Earth System' (project no. 49926684) and EXC 2077 'The Ocean Floor—Earth's Uncharted Interface' (project no. 390741601). Funding for M. Rubin-Blum was provided by the Israel Science Foundation (913/19), the U.S.-Israel Binational Science Foundation (2019055) and the Israel Ministry of Science and Technology (1126). H. Vigderovich was supported by a student fellowship from the Israel Water Authority.

References

Adler, Michal, Eckert, W., & Sivan, O. (2011). Quantifying rates of methanogenesis and methanotrophy in Lake Kinneret sediments (Israel) using porewater profiles. *Limnology and Oceanography*, *56*(4), 1525–1535. https://doi.org/10.4319/lo.2011.56.4.1525

Aepfler, R. F., Bühring, S. I., & Elvert, M. (2019). Substrate characteristic bacterial fatty acid production based on amino acid assimilation and transformation in marine sediments. *FEMS Microbiology Ecology*, *95*(10), 1–15. https://doi.org/10.1093/femsec/fiz131

Amiel, N. (2018). *Authigenic magnetite in deep sediments.* MsC thesis, Ben Gurion University of the Negev.

Arshad, A., Speth, D. R., De Graaf, R. M., Op den Camp, H. J. M., Jetten, M. S. M., & Welte, C. U. (2015). A metagenomics-based metabolic model of nitrate-dependent anaerobic oxidation of methane by Methanoperedens-like archaea. *Frontiers in Microbiology*, *6*(DEC), 1–14. https://doi.org/10.3389/fmicb.2015.01423

Bai, Y. N., Wang, X. N., Wu, J., Lu, Y. Z., Fu, L., Zhang, F., Lau, TC., & Zeng, R. J. (2019). Humic substances as electron acceptors for anaerobic oxidation of methane driven by ANME-2d. *Water Research*, *164*,

114935. https://doi.org/10.1016/j.watres.2019.114935

Bankevich, A., Nurk, S., Antipov, D., Gurevich, A. a., Dvorkin, M., Kulikov, A. S., Lesin, V. M., Nicolenko, S. I., Pham, S., Prjibelski, A. D., Sirotkin, A. V., Vyahhi, N., Tesler, G., Aleksyev, A. M., & Pevzner, P. a. (2012). SPAdes: A New Genome Assembly Algorithm and Its Applications to Single-Cell Sequencing. *Journal of Computational Biology*, *19*(5), 455–477. https://doi.org/10.1089/cmb.2012.0021

Bar-Or, I., Ben-Dov, E., Kushmaro, A., Eckert, W., & Sivan, O. (2015). *Methane-related changes in prokaryotes along geochemical profiles in sediments of Lake Kinneret (Israel) Methane-related changes in prokaryotes along geochemical profiles in sediments of Lake Kinneret (Israel)*. (August). https://doi.org/10.5194/bg-12-2847-2015

Bar-Or, I., Elvert, M., Eckert, W., Kushmaro, A., Vigderovich, H., Zhu, Q., Ben-Dov, E., & Sivan, O. (2017). Iron-Coupled Anaerobic Oxidation of Methane Performed by a Mixed Bacterial-Archaeal Community Based on Poorly Reactive Minerals. *Environmental Science & Technology*, *51*, 12293–12301. https://doi.org/10.1021/acs.est.7b03126

Bastviken D. (2009). Methane. In: Likens G.E., ed. Encyclopedia of Inland waters, Oxford: Elsevier, 783–805. http://doi.org/10.1016/B978-012370626-3.00117-4.

Beck, D. A. C., Kalyuzhnaya, M. G., Malfatti, S., Tringe, S. G., del Rio, T. G., Ivanova, N., Lidstorm, M. E., & Chistoserdova, L. (2013). A metagenomic insight into freshwater methane-utilizing communities and evidence for cooperation between the Methylococcaceae and the Methylophilaceae. *PeerJ*, *2013*(1), 1–23. https://doi.org/10.7717/peerj.23

Biderre-Petit, C., Dugat-Bony, E., Mege, M., Parisot, N., Adrian, L., Moné, A., Denonfoux, J., Peyretaillade, E., Debroas. D., Boucher, D., Peyret, P. (2016). Distribution of Dehalococcoidia in the anaerobic deep water of a remote meromictic crater lake and detection of Dehalococcoidia-derived reductive dehalogenase homologous genes. *PLoS ONE*, *11*(1), 1–19. https://doi.org/10.1371/journal.pone.0145558

Boetius, A., Ravenschlag, K., Schubert, C. J., Rickert, D., Widdel, F., Gieseke, A., Amann, R., Jørgensen, B.B., Witte, U., & Pfannkuche, O. (2000). A marine microbial consortium apparently mediating AOM. *Nature*, *407*(October), 623–626.

Bottrell, S. H., Parkes, R. J., Cragg, B. A., & Raiswell, R. (2000): Isotopic evidence for anoxic pyrite oxidation and stimulation of bacterial sulphate reduction in marine sediments, *J. Geol. Soc. London*,157, 711–714. https://doi.org/10.1144/jgs.157.4.711.

Cabrol, L., Thalasso, F., Gandois, L., Sepulveda-Jauregui, A., Martinez-Cruz, K., Teisserenc, R., Tananaev, N., Tveit, A., Svenning, M. M., & Barret, M. (2020). Anaerobic oxidation of methane and associated microbiome in anoxic water of Northwestern Siberian lakes. *Science of the Total Environment*, *736*, 139588. https://doi.org/10.1016/j.scitotenv.2020.139588

Cai, C., Leu, A. O., Xie, G-J., Guo, J., Feng, Y., Zhao, J-X., Tyson, G. W., Yuan, Z., & Hu, S. (2018). A

methanotrophic archaeon couples anaerobic oxidation of methane to Fe(II) reduction. ISME J, 12, 1929-1939. http://dx.doi.org/10.1038/s41396-018-0109-x

Cheng, L., Shi, S. bao, Yang, L., Zhang, Y., Dolfing, J., Sun, Y. ge, Liu, L., Li, Q., Tu, B., Dai, L., Shi, Q., & Zhang, H. (2019). Preferential degradation of long-chain alkyl substituted hydrocarbons in heavy oil under methanogenic conditions. *Organic Geochemistry*, *138*. https://doi.org/10.1016/j.orggeochem.2019.103927

Chuang, P. C., Yang, T. F., Wallmann, K., Matsumoto, R., Hu, C. Y., Chen, H. W., Lin, S., Sun, CH., Li, HC., Wang, Y., & Dale, A. W. (2019). Carbon isotope exchange during anaerobic oxidation of methane (AOM) in sediments of the northeastern South China Sea. *Geochimica et Cosmochimica Acta*, *246*, 138–155. https://doi.org/10.1016/j.gca.2018.11.003

Clement, J-C., Shrestha, J., Ehrenfeld, J. G., & Jaffe, P. R. (2005). Ammonium oxidation coupled to dissimilatory iron reduction under anaerobic conditions in wetland soils. *Soil biology and biochemistry, 37(12),* 2323-2328. http://doi.org/10.1016/j.soilbio.2005.03.027

Conrad, R. (2009). The global methane cycle: Recent advances in understanding the microbial processes involved. *Environmental Microbiology Reports*, *1*(5), 285–292. https://doi.org/10.1111/j.1758-2229.2009.00038.x

Crowe, S. A., Katsev, S., Leslie, K., Sturm, A., Magen, C., Nomosatryo, S., Pack, M. A., Kessler, J. D., Reeburgh, W. S., Roberts, J. a., González, L., Douglas Haffner, G., Mucci, A., Sundby, B., & Fowle, D. A. (2011). The methane cycle in ferruginous Lake Matano. *Geobiology, 9(1)*, 61-78. http://doi.org/10.1111/j.1472-4669.2010.00257.x

Damgaard, L. R., Revsbech, N. P., & Reichardt, W. (1998). Use of an oxygen-insensitive microscale biosensor for methane to measure methane concentration profiles in a rice paddy. *Applied and Environmental Microbiology, 64(3)*, 864-870. http://doi.org/10.1128/aem.64.3.864-870.1998

Dershwitz, P., Bandow, N. L., Yang, J., Semrau, J. D., McEllistrem, M. T., Heinze, R. A., Fonseca, M., Ledesma, J. C., Jennett, J. R., DiSpirito, A. M., Athwal, N. S., Hargrove, M. S., Bobik, T. A., Zischka, H., & DiSpirito, A. A. (2021). Oxygen Generation via Water Splitting by a Novel Biogenic Metal Ion-Binding Compound. *Applied and Environmental Microbiology*, *87*(14), 1–14. https://doi.org/10.1128/aem.00286-21

Ding, L. J., An, X. L., Li, S., Zhang, G. L., & Zhu, Y. G. (2014). Nitrogen loss through anaerobic ammonium oxidation coupled to iron reduction from paddy soils in a chronosequence. *Environmental Science and Technology, 48(18)*, 10641-10647. http://doi.org/10.1021/es503113s

Elul, M., Rubin-Blum, M., Ronen, Z., Bar-Or, I., Eckert, W., & Sivan, O. (2021). Metagenomic insights into the metabolism of microbial communities that mediate iron and methane cycling in Lake Kinneret sediments. *Biogeosciences Discussions*, 1–24. https://doi.org/10.5194/bg-2020-329

Elvert, M., Boetius, A., Knittel, K., & Jørgensen, B. B. (2003). Characterization of specific membrane fatty acids as chemotaxonomic markers for sulfate-reducing bacteria involved in anaerobic oxidation of methane. *Geomicrobiology Journal*, *20*(4), 403–419. https://doi.org/10.1080/01490450303894

Ettwig, K. F., Zhu, B., Speth, D., Keltjens, J. T., Jetten, M. S. M., & Kartal, B. (2016). Archaea catalyze iron-

dependent anaerobic oxidation of methane. *PNAS, 113(45)*, 12792-12796. http://doi.org/10.1073/pnas.1609534113

Ettwig, Katharina F, Butler, M. K., Le Paslier, D., Pelletier, E., Mangenot, S., Kuypers, M. M. M., Schreiber, F., Dutilh, B. E., Zedelius, J., de Beer, D. Gloerich, J., Wessels, H. J. C. T., van Alen, T., Luesken, F., Wu, M. L., van de Pas-Schoonen K. T., Op den Camp, H. J. M., Jansen-Megens, E. M., Francojs, KJ., Stunnenberg, H., Weissenbach, J., Jetten, M. S. M., & Strous, M. (2010). Nitrite-driven anaerobic methane oxidation by oxygenic bacteria. *Nature*, *464*(7288), 543–548. https://doi.org/10.1038/nature08883

Evans, P. N., Parks, D. H., Chadwick, G. L., Robbins, S, J., Orphan V. J., Golding, S. D., & Tyson, G. W. (2015). *Science*. 350(6259), 434-438. http://doi.org/ 10.1126/science.aac7745.

Fan, L., Dippold, M. A., Ge, T., Wu, J., Thiel, V., Kuzyakov, Y., & Dorodnikov, M. (2020). Anaerobic oxidation of methane in paddy soil: Role of electron acceptors and fertilization in mitigating CH4 fluxes. *Soil Biology and Biochemistry*, *141*, 107685. https://doi.org/10.1016/j.soilbio.2019.107685

Froelich, P. N., Klinkhammer, G. P., Lender, M. L., Luedtke, N. A., Heath, G. R., Cullen, D., Dauphin, P., Hammond, D., Hartman, B., & Maynard, V. (1979). *Geochemica et Cosmochimica Acta, 43*, 1075-1090. https://doi.org/10.1016/0016-7037(79)90095-4

Gropp, J., Iron, M. A., & Halevy, I. (2021). Theoretical estimates of equilibrium carbon and hydrogen isotope effects in microbial methane production and anaerobic oxidation of methane. *Geochimica et Cosmochimica Acta*, *295*, 237–264. https://doi.org/10.1016/j.gca.2020.10.018

Hallam, S. J., Putnam, N., Preston, C. M., Detter, J. C., Rokhsar, D., Richardson, P. H., & DeLong, E. F. (2004). Reverse methanogenesis: Testing the hypothesis with environmental genomics. *Science*, *305*(5689), 1457–1462. https://doi.org/10.1126/science.1100025

Hammer, Ø., Harper, D. A. T., & Ryan, P. D. (2001) Past: paleontological statistics software package for education and data analysis. *Paleontologia-Electronica*. 4 (1), 9.

Haroon, M. F., Hu, S., Shi, Y., Imelfort, M., Keller, J., Hugenholtz, P., Yuan, Z., & Tyson, G. W. (2013). Anaerobic oxidation of methane coupled to nitrate reduction in a novel archaeal lineage. *Nature*, *500*(7464), 567–570. https://doi.org/10.1038/nature12375

Hoehler, T. M., Alperin, M. J., Albert, D. B., & Martens, C. S. (1994). Field and laboratory, evidence for a methane-sulfate reducer consortium.pdf. *Global Biogeochemical Cycles*, *8*(4), 451–463.

Holler, T., Wegener, G., Niemann, H., Deusner, C., Ferdelman, T. G., Boetius, A., Brunner, B., & Widdel, F. (2011). Carbon and sulfur back flux during anaerobic microbial oxidation of methane and coupled sulfate reduction. *Proceedings of the National Academy of Sciences of the United States of America*, *108*(52). https://doi.org/10.1073/pnas.1106032108

Holmkvist, L., Ferdelman, T. G., & Jørgensen, B. B. (2011). A cryptic sulfur cycle driven by iron in the methane zone of marine sediment (Aarhus Bay, Denmark). *Geochimica et Cosmochimica Acta*, *75*(12), 3581–3599. https://doi.org/10.1016/j.gca.2011.03.033

761 Hug, L. A., Castelle, C. J., Wrighton, K. C., Thomas, B. C., Sharon, I., Frischkorn, K. R., Williams, K. H.,
762 Tringe, S. G., & Banfield, J. F. (2013). Community genomic analyses constrain the distribution of
763 metabolic traits across the Chloroflexi phylum and indicate roles in sediment carbon cycling. *Microbiome*,
764 *1*(1), 1–17. https://doi.org/10.1186/2049-2618-1-22

765 Kang, D. D., Li, F., Kirton, E., Thomas, A., Egan, R., An, H., & Wang, Z. (2019). MetaBAT 2: An adaptive
766 binning algorithm for robust and efficient genome reconstruction from metagenome assemblies. *PeerJ*,
767 *2019*(7), 1–13. https://doi.org/10.7717/peerj.7359

768 Kellermann, M. Y., Wegener, G., Elvert, M., Yoshinaga, M. Y., Lin, Y. S., Holler, T., Mollar, P. X., Knittel K.,
769 & Hinrichs, K. U. (2012). Autotrophy as a predominant mode of carbon fixation in anaerobic methane-
770 oxidizing microbial communities. *Proceedings of the National Academy of Sciences of the USA* 109(47),
771 19321-19326. doi:10.1073/pnas.1208795109.

772 Kits, K. D., Klotz, M. G., & Stein, L. Y. (2015). Methane oxidation coupled to nitrate reduction under hypoxia
773 by the Gammaproteobacterium Methylomonas denitrificans, sp. nov. type strain FJG1. *Environmental*
774 *Microbiology*, *17*(9), 3219–3232. https://doi.org/10.1111/1462-2920.12772

775 Knittel, K., & Boetius, A. (2009). Anaerobic oxidation of methane: Progress with an unknown process. *Annual*
776 *Review of Microbiology*, *63*, 311–334. https://doi.org/10.1146/annurev.micro.61.080706.093130

777 Kurth, J.M., Nadine T Smit, Stefanie Berger, Stefan Schouten, Mike S M Jetten, Cornelia U Welte, Anaerobic
778 methanotrophic archaea of the ANME-2d clade feature lipid composition that differs from other ANME
779 archaea, FEMS Microbiology Ecology, Volume 95, Issue 7, July 2019, fiz082.

780 Li, X., Hou, L., Liu, M., Zheng, Y., Yin, G., Lin, X., Cheng, L., Li, Y., & Hu, X. (2015). Evidence of Nitrogen
781 Loss from Anaerobic Ammonium Oxidation Coupled with Ferric Iron Reduction in an Intertidal Wetland.
782 *Environmental Science and Technology*, *49*(19), 11560–11568. https://doi.org/10.1021/acs.est.5b03419

783 Lin, Y. S., Lipp, J. S., Yoshinaga, M. Y., Lin, S. H., Elvert, M., & Hinrichs, K. U. (2010). Intramolecular stable
784 carbon isotopic analysis of archaeal glycosyl tetraether lipids. *Rapid Communications in Mass*
785 *Spectrometry*, *24*(19), 2817–2826. https://doi.org/10.1002/rcm.4707Lovley, D. R., & Klug, M. J. (1983).
786 Sulfate reducers can outcompete methanogens at freshwater sulfate concentrations. *Applied and*
787 *Environmental Microbiology*, *45*(1), 187–192. https://doi.org/10.1128/aem.45.1.187-192.1983

788 Lovely, D. R., Coates, J. D., Blunt-Harris, E. L., Phillips, E. J. P., & Woodward, J. C. (1996). Humic substances
789 as electron acceptors for microbial respiration. *Nature, 382*, 445-448. https://doi.org/10.1038/382445a0

790 Lu, Y. Z., Fu, L., Ding, J., Ding, Z. W., Li, N., & Zeng, R. J. (2016). Cr(VI) reduction coupled with anaerobic
791 oxidation of methane in a laboratory reactor. *Water Research, 102*, 445-452.
792 http://doi.org/10.1016/j.watres.2016.06.065

793 Martinez-cruz, K., Leewis, M., Charold, I., Sepulveda-jauregui, A., Walter, K., Thalasso, F., & Beth, M. (2017).
794 Science of the Total Environment Anaerobic oxidation of methane by aerobic methanotrophs in sub-
795 Arctic lake sediments. *Science of the Total Environment*, *607–608*, 23–31.
796 https://doi.org/10.1016/j.scitotenv.2017.06.187

797 Meador, T. B., Gagen, E. J., Loscar, M. E., Goldhammer, T., Yoshinaga, M. Y., Wendt, J., Thomm, M., &
798 Hinrichs, K. U. (2014). Thermococcus kodakarensis modulates its polar membrane lipids and elemental
799 composition according to growth stage and phosphate availability. *Frontiers in Microbiology*, *5*(JAN), 1–
800 13. https://doi.org/10.3389/fmicb.2014.00010

801 Meister, P., Liu, B., Khalili, A., Böttcher, M. E., & Jørgensen, B. B. (2019). Factors controlling the carbon
802 isotope composition of dissolved inorganic carbon and methane in marine porewater: An evaluation by
803 reaction-transport modelling. *Journal of Marine Systems*, *200*(August), 103227.
804 https://doi.org/10.1016/j.jmarsys.2019.103227

805 Moran, J. J., House, C. H., Freeman, K. H., & Ferry, J. G. (2005). Trace methane oxidation studied in several
806 Euryarchaeota under diverse conditions. *Archaea*, *1*(5), 303–309. https://doi.org/10.1155/2005/650670

807 Mosrovaya, A., Wind-Hansen, M., Rousteau, P., Bristow, L. A., & Thamdrup, B. (2021) Sulfate- and iron-
808 dependent anaerobic methane oxidation occuring side-by-side in freshwater lake sediments. *Limnology*
809 *and Oceanography*. https://doi.org/10.1002/lno.11988

810 Nollet, L., Demeyer, D., & Verstraete, W. (1997). Effect of 2-bromoethanesulfonic acid and Peptostreptococcus
811 productus ATCC 35244 addition on stimulation of reductive acetogenesis in the ruminal ecosystem by
812 selective inhibition of methanogenesis. *Applied and Environmental Microbiology*, *63*(1), 194–200.
813 https://doi.org/10.1128/aem.63.1.194-200.1997

814 Norði, K á., Thamdrup B., & Schubert, C. J. (2013). Anaerobic oxidation of methane in an iron-rich Danish
815 freshwater lake sediment. *Limnology and Oceanography, 58(2)*, 546-554.
816 http://doi.org/10.4319/lo.2013.58.2.0546

817 Norði, K á., & Thamdrup B. (2014). Nitrate-dependent anaerobic methane oxidation in freshwater sediment.
818 *Geochimica et Cosmochimica Acta, 132*, 141-150. http://doi.org/10.1016/j.gca.2014.01.032

819 Nurk, S., Bankevich, A., & Antipov, D. (2013). Assembling genomes and mini-metagenomes from highly
820 chimeric reads. *Research in Computational Molecular Biology*, 158–170. https://doi.org/10.1007/978-3-
821 642-37195-0

822 Nüsslein, B., Chin, K. J., Eckert, W., & Conrad, R. (2001). Evidence for anaerobic syntrophic acetate oxidation
823 during methane production in the profundal sediment of subtropical Lake Kinneret (Israel). *Environmental*
824 *Microbiology*, *3*(7), 460–470. https://doi.org/10.1046/j.1462-2920.2001.00215.x

825 Orembland, R. S., & Capone, D. G. (1988). *Use of "Specific" Inhibitors in Biogeochemistry and Microbial*
826 *Ecology* (Vol. 10). https://doi.org/10.2307/4514

827 Orphan, V. J., House, C. H., & Hinrichs, K. (2001). Methane-Consuming Archaea Revealed by Directly
828 Coupled Isotopic and Phylogenetic Analysis. *Science*, *293*(July), 484–488.
829 https://doi.org/10.1126/science.1061338

830 Oswald, K., Milucka, J., Brand, A., Hach, P., Littmann, S., Wehrli, B., Albersten, M., Daims, H., Wagner, M.,
831 Kuypers, M. M. M., Schubert, C. J., & Milucka, J. (2016). Aerobic gammaproteobacterial methanotrophs

mitigate methane emissions from oxic and anoxic lake waters. *Limnology and Oceanography*, *61*, S101–S118. https://doi.org/10.1002/lno.10312

Parks, D. H., Chuvochina, M., Rinke, C., Mussig, A. J., Chaumeil, P-A., & Hugenholtz, P. (2021) GTDB: an ongoing census of bacterial and archaeal diversity through a phylogenetically consistent, rank normalized and complete genome-based taxonomy. *Nucleic Acids Research, 202, 1-10.* http://doi.org/10.1093/nar/gkab776

Raghoebarsing, A. A., Pol, A., Van De Pas-Schoonen, K. T., Smolders, A. J. P., Ettwig, K. F., Rijpstra, W. I. C., Schouten, S., Sinninghe Damsté, J. S., Op den Camp, H. J. M., Jetten, M. S. M., & Strous, M. (2006). A microbial consortium couples anaerobic methane oxidation to denitrification. *Nature*, *440*(7086), 918–921. https://doi.org/10.1038/nature04617

Reeburgh, W. S. (2007). Oceanic Methane Biogeochemistry. *ChemInform*, *38*(20), 486–513. https://doi.org/10.1002/chin.200720267

Rosentreter, J. A., Borges, A. V., Deemer, B. R., Holgerson, M. A., Liu, S., Song, C., Melack, J., Raymond, P. A., Duarte, C. M., Allen, G. H., Olefeldt, D., Poulter, B., Battin, T. I., & Eyre, B. D. (2021). *Nature geoscience, 14(4)*, 225-230. http://doi.org/ 10.1038/s41561-021-00715-2

Saunois, M., Stavert, A. R., Poulter, B., Bousquet, P., Canadell, J. G., Jackson, R. B., Raymond, P. A., Dlugokencky, E. J., Houweling, S., Patra, P. K., Ciais, P., Arora, V. K., Bastviken, D., Bergamaschi, P., Blake, D. R., Brailsford, G., Bruhwiler, L., Carlson, K. M., Carrol, M., Castaldi, S., Chandra, N., Crevoisier, C., Crill, P. M., Covey, K., Curry, C. L., Etiope, G., Frankenberg, C., Gedney, N., Hegglin, M. I., Höglund-Isaksson, L., Hugelius, G., Ishizawa, M., Ito, A., Janssens-Maenhout, G., Jensen, K. M., Joos, F., Kleinen, T., Krummel, P. B., Langenfelds, R. L., Laruelle, G. G., Liu, L., Machida, T., Maksyutov, S., McDonald, K. C., McNorton, J., Miller, P. A., Melton, J. R., Morino, I., Müller, J., Murguia-Flores, F., Naik, V., Niwa, Y., Noce, S., O'Doherty, S., Parker, R. J., Peng, C., Peng, S., Peters, G. P., Prigent, C., Prinn, R., Ramonet, M., Regnier, P., Riley, W. J., Rosentreter, J. A., Segers, A., Simpson, I. J., Shi, H., Smith, S. J., Steele, L. P., Thornton, B. F., Tian, H., Tohjima, Y., Tubiello, F. N., Tsuruta, A., Viovy, N., Voulgarakis, A., Weber, T. S., van Weele, M., van der Werf, G. R., Weiss, R. F., Worthy, D., Wunch, D., Yin, Y., Yoshida, Y., Zhang, W., Zhang, Z., Zhao, Y., Zheng, B., Zhu, Q., Zhu, Q., and Zhuang, Q.: The Global Methane Budget 2000–2017, Earth Syst. Sci. Data, 12, 1561–1623, https://doi.org/10.5194/essd-12-1561-2020, 2020.

Schubert, C. J., Vazquez, F., Lösekann-Behrens, T., Knittel, K., Tonolla, M., & Boetius, A. (2011). Evidence for anaerobic oxidation of methane in sediments of a freshwater system (Lago di Cadagno). *FEMS Microbiology Ecology, 76(1)*, 26-38. http://doi.org/ 10.1111/j.1574-6941.2010.01036.x

Segarra, K. E. A., Schubotz, F., Samarkin, V., Yoshinaga, M. Y., Hinrichs, K-U., & Joye, S. B. (2015). *Nature communications, 6(may)*, 1-8. http://dx.doi.org/10.1038/ncomms8477

Sela-Adler, M., Herut, B., Bar-Or, I., Antler, G., Eliani-Russak, E., Levy, E., Makovsky, Y., & Sivan, O. (2015). Geochemical evidence for biogenic methane production and consumption in the shallow sediments of the SE Mediterranean shelf (Israel). *Continental Shelf Research*, *101*, 117–124. https://doi.org/10.1016/j.csr.2015.04.001

Shrestha, J., Rich, J. J., Ehrenfeld, J. G., & Jaffe, P. R. (2009). Oxidation of ammonium to nitrite under iron-reducing conditions in wetland soils: Laboratory, field demonstrations, and push-pull rate determination. *Soil Science, 174(3)*, 156-164. http://doi.org/10.1097/SS.0b013e3181988fbf

Shuai, W., & Jaffé, P. R. (2019). Anaerobic ammonium oxidation coupled to iron reduction in constructed wetland mesocosms. *Science of the Total Environment*, *648*, 984–992. https://doi.org/10.1016/j.scitotenv.2018.08.189

Sieber, C. M. K., Probst, A. J., Sharrar, A., Thomas, B. C., Hess, M., Tringe, S. G., & Banfield, J. F. (2018). Recovery of genomes from metagenomes via a dereplication, aggregation and scoring strategy. *Nature Microbiology*, *3*(7), 836–843. https://doi.org/10.1038/s41564-018-0171-1

Sinke, A. J.C., Cornelese, A. A., Cappenberg, T. E., & Zehnder, A. J. B. (1992). Seasonal variation in sulfate reduction and methanogenesis in peaty sediments of eutrophic Lake Loosdrecht, The Netherlands. *Biogeochemistry, 16(1)*, 43-61. http://doi.org/10.1007/BF02402262

Sivan, O, Adler, M., Pearson, A., Gelman, F., Bar-Or, I., John, S. G., & Eckert, W. (2011). Geochemical evidence for iron-mediated anaerobic oxidation of methane. *Limnology and Oceanography*, *56*(4), 1536–1544.

Stookey, L. L. (1970). Ferrozine-a new spectrophotometric reagent for iron. *Analytical Chemistry*, *42*(7), 779–781. https://doi.org/10.1021/ac60289a016

Sturt, H. F., Summons, R. E., Smith, K., Elvert, M., & Hinrichs, K. U. (2004). Intact polar membrane lipids in prokaryotes and sediments deciphered by high-performance liquid chromatography/electrospray ionization multistage mass spectrometry - New biomarkers for biogeochemistry and microbial ecology. *Rapid Communications in Mass Spectrometry*, *18*(6), 617–628. https://doi.org/10.1002/rcm.1378

Su, G., Zopfi, J., Yao, H., Steinle, L., Niemann, H., & Lehmann, M. F. (2020). Manganese/iron-supported sulfate-dependent anaerobic oxidation of methane by archaea in lake sediments. *Limnology and Oceanography*, *65*(4), 863–875. https://doi.org/10.1002/lno.11354

Tamames, J., & Puente-Sánchez, F. (2019). SqueezeMeta, A Highly Portable, Fully Automatic Metagenomic Analysis Pipeline. *Frontiers in Microbiology*, *9*. https://doi.org/10.3389/fmicb.2018.03349

Tan, X., Xie, G. J., Nie, W. B., Xing, D-F., Liu, B. F., Ding, J., & Ren, N. Q. (2021). Fe(III)-mediated anaerobic ammonium oxidation: A novel microbial nitrogen cycle pathway and potential applications. *Critical Reviews in Environmental Science and Technology*. https://doi.org/10.1080/10643389.2021.1903788

Timmers, P. H. A., Welte, C. U., Koehorst, J. J., Plugge, C. M., Jetten, M. S. M., & Stams, A. J. M. (2017). Reverse Methanogenesis and Respiration in Methanotrophic Archaea. *Archaea*, *2017*(Figure 1). https://doi.org/10.1155/2017/1654237

Treude, T., Krause, S., Maltby, J., Dale, A. W., Coffin, R., & Hamdan, L. J. (2014). Sulfate reduction and methane oxidation activity below the sulfate-methane transition zone in Alaskan Beaufort Sea continental margin sediments: Implications for deep sulfur cycling. *Geochimica et Cosmochimica Acta*, *144*, 217–237. https://doi.org/10.1016/j.gca.2014.08.018

906 Treude, T., Niggemann, J., Kallmeyer, J., Wintersteller, P., Schubert, C. J., Boetius, A., & Jørgensen, B. B.
907 (2005). Anaerobic oxidation of methane and sulfate reduction along the Chilean continental margin.
908 *Geochimica et Cosmochimica Acta*, *69*(11), 2767–2779. https://doi.org/10.1016/j.gca.2005.01.002

909 Valentine D. L. (2002). Biogeochemistry and microbial ecology of methane oxidation in anoxic environments:
910 A review. Antonie van Leeuwenhoek, 81(1-4), 271-282. http://doi.org/ 10.1023/A:1020587206351

911 Valenzuela, E. I., Avendaño, K. A., Balagurusamy, N., Arriaga, S., Nieto-Delgado, C., Thalasso, F., &
912 Cervantes, F. J. (2019). Electron shuttling mediated by humic substances fuels anaerobic methane
913 oxidation and carbon burial in wetland sediments. *Science of the Total Environment*, *650*, 2674–2684.
914 https://doi.org/10.1016/j.scitotenv.2018.09.388

915 Valenzuela, E. I., Prieto-Davó, A., López-Lozano, N. E., Hernández-Eligio, A., Vega-Alvarado, L., Juárez, K.,
916 García-González, A. S., López, M. G., & Cervantes, F. J. (2017). Anaerobic methane oxidation driven by
917 microbial reduction of natural organic matter in a tropical wetland. *Applied and Environmental*
918 *Microbiology*, *83*(11), 1–15. https://doi.org/10.1128/AEM.00645-17

919 Vigderovich, H., Liang, L., Herut, B., Wang, F., Wurgaft, E., Rubin-Blum, M., & Sivan, O. (2019). Evidence
920 for microbial iron reduction in the methanogenic sediments of the oligotrophic SE Mediterranean
921 continental shelf. *Biogeosciences Discussions*, 1–25. https://doi.org/10.5194/bg-2019-21

922 Wang, L., Miao, X., Ali, J., Lyu, T., & Pan, G. (2018). Quantification of Oxygen Nanobubbles in Particulate
923 Matters and Potential Applications in Remediation of Anaerobic Environment. *ACS Omega*, *3*(9), 10624–
924 10630. https://doi.org/10.1021/acsomega.8b00784

925 Wegener G, Niemann H, Elvert M, Hinrichs K-U, Boetius A (2008). Assimilation of methane and inorganic
926 carbon by microbial communities mediating the anaerobic oxidation of methane. Environmental
927 Microbiology 10(9), 2287-2298. doi: 10.1111/j.1462-2920.2008.01653.x.

928 Wegener, G., Gropp, J., Taubner, H., Halevy, I., & Elvert, M. (2021). Sulfate-dependent reversibility of
929 intracellular reactions explains the opposing isotope effects in the anaerobic oxidation of methane. *Science*
930 *Advances*, *7*(19), 1–14. https://doi.org/10.1126/sciadv.abe4939

931 Whiticar, M. J., Faber, E., & Schoell, M. (1986). Biogenic methane formation in marine and freshwater
932 environments: CO2 reduction vs. acetate fermentation-Isotope evidence. Geochimica et Cosmochimica
933 Acta, 50(5), 693-709. http://doi.org/ 10.1016/0016-7037(86)90346-7

934 Wu, Y.W., Tang, Y.-H., Tringe, S. G., Simmons, B. A., & Singer, S. W. (2014). MaxBin: an automated binning
935 method to recover individual genomes from metagenomes using. *Microbiome*, *2*(26), 4904–4909.
936 Retrieved from https://microbiomejournal.biomedcentral.com/articles/10.1186/2049-2618-2-26

937 Wuebbles, D. J., & Hayhoe, K. (2002). Atmospheric methane and global change. *Earth-Science Reviews*, *57*(3–
938 4), 177–210. https://doi.org/10.1016/S0012-8252(01)00062-9

939 Xu, Z., Masuda, Y., Wang, X., Ushijima, N., Shiratori, Y., Senoo, K., & Itoh, H. (2021). Genome-Based

940 Taxonomic Rearrangement of the Order Geobacterales Including the Description of Geomonas
941 azotofigens sp. nov. and Geomonas diazotrophica sp. nov. Frontiers in Microbiology, 12(September).
942 http://doi.org/ 10.3389/fmicb.2021.737531

943 Yorshansky, O. (2019). *Iron Reduction in Deep Marine Sediments of the Eastern Mediterranean Continental*
944 *Shelf and the Yarqon Estuary*. MsC thesis, Ben Gurion University of the Negev.

945 Yoshinaga, M. Y., Holler, T., Goldhammer, T., Wegener, G., Pohlman, J. W., Brunner, B., Kuypers, M. M. M.,
946 Hinrichs, K. U., & Elvert, M. (2014). Carbon isotope equilibration during sulphate-limited anaerobic
947 oxidation of methane. *Nature Geoscience*, *7*(3), 190–194. https://doi.org/10.1038/ngeo2069

948 Zehnder, a J., & Brock, T. D. (1979). Methane formation and methane oxidation by methanogenic bacteria.
949 *Journal of Bacteriology*, *137*(1), 420–432.

950 Zhang, X., Xia, J., Pu, J., Cai, C., Tyson, G. W., Yuan, Z., & Hu, S. (2019). Biochar-Mediated Anaerobic
951 Oxidation of Methane. *Environmental Science and Technology*, *53*(12), 6660–6668.
952 https://doi.org/10.1021/acs.est.9b01345

953 Zheng, Y., Wang, H., Liu, Y., Zhu, B., Li, J., Yang, Y., Qin, W., Chen, L., Wu, X., Chistoserdova, L., & Zhao,
954 F. (2020). Methane-Dependent Mineral Reduction by Aerobic Methanotrophs under Hypoxia.
955 *Environmental Science and Technology Letters*, *7*(8), 606–612. https://doi.org/10.1021/acs.estlett.0c00436

956